QATAR UNIVERSITY

COLLEGE OF ENGINEERING

THE EFFECT OF GROOVING, EXTERNAL, AND INTERNAL GFRP OVERWRAPPED PVC TUBES ON CRASHWORTHINESS CHARACTERISTICS

BY

KHALED Y. ALI

A Thesis Submitted to

the College of Engineering

in Partial Fulfillment of the Requirements for the Degree of

Masters of Science in Mechanical Engineering

June 2022

COMMITTEE PAGE

The members of the Committee approve the Thesis of
Khaled Y. Ali defended on 12/05/2022.

Prof. Elsadig Mahdi Saad
Thesis Supervisor

Dr. John-John Cabibihan
Program Coordinator

Dr. Faris Tarlochan
Committee Member

Dr. Anwar Hasan
Committee Member

Prof. Mohd Sapuan Salit
Committee Member

Approved:

Khalid Kamal Naji, Dean, College of Engineering

ABSTRACT

ALI, KHALED, Y., Masters: June : 2022, Masters of Science in Mechanical Engineering

Title: The Effect of Grooving, External, and Internal GFRP Overwrapped PVC Tube on Crashworthiness Characteristics

Supervisor of Thesis: Elsadig M. Saad.

Several factors that affect the crashworthiness characteristics were investigated using GFRP overwrapped PVC composite tubes. Composite tubes studied alongside the PVC were non-grooved tubes wrapped externally or internally, and the same for the grooved tubes. All tubes underwent a quasi-static axial compression test. All composite samples had a capacity of load-bearing, a capability to absorb energy, and a crushing force efficiency significantly higher than the PVC. The grooved specimen wrapped externally only had the best amount of SEA compared to other tested tubes by an average of 17.5 kJ/kg for pre and post-crushing stages combined. However, its crushing failure was not stable, presenting poor CFE and lowest iCFE among the composite tubes by an average of 43.59%. The advantage of grooving was observed in increasing the initial peak load for the grooved composite tubes, which provided a substantial rise in the capability of absorbing energy in the pre-crushing stage without disturbing the stability of CFE. Meanwhile, the advantage of wrapping externally and internally was enhancing CFE and iCFE. Therefore, the composite tube that combines grooving and wrapping externally and internally got the highest rank in the best performing selection among all the tested tubes.

DEDICATION

This thesis is dedicated to my family. They always supported and motivated me with their warm prayers and kind words to achieve my goals. Many thanks are devoted to my supervisor Prof. Elsadig Saad who helped and supported me since the first day of my master's journey. Thank you all for being in my life. Without your support and guidance, I would not be able to achieve this success.

ACKNOWLEDGMENTS

This thesis was accomplished at Qatar University in the Department of Mechanical and Industrial Engineering. The writer enormously appreciates the support provided by all university faculty members during the period of writing this thesis.

The author would like to thank Prof. Elsadig for his considerable support and supervision while working on this thesis.

TABLE OF CONTENTS

LIST OF TABLES

LIST OF FIGURES

CHAPTER 1: INTRODUCTION

This section includes a short background about the studied obstacle followed by the research objectives and significance. In addition, the overall thesis outline will be introduced at the end of this chapter.

1.1. Background

Crashworthiness is identified as the vehicle's resistance in case of a collision to protect the passengers [1]. According to World Health Organization (WHO), an average of 1.35 million deaths around the world due to traffic crashes every year. Making vehicle crashes the eighth leading cause of death globally and the leading cause of death for people aged between 5-29 years [2]. Accordingly, crashworthiness is considered an important parameter for vehicles, making it a research topic. Efforts have been devoted to designing vehicles that can absorb maximum energy while maintaining sufficient survivability for occupants [3].

Mass, volume, and increased fuel efficiency should all be considered while designing vehicles to ensure a certain level of protection. In addition, composite materials' properties, such as corrosion, fatigue resistance, high strength ratios, and stiffness to weight, make them desirable for crashworthiness applications. As a result, various metal parts in automobiles have been replaced with composite materials. The challenge is to manufacture lightweight vehicles using specific geometry while maintaining the safety and economic feasibility of the design [4].

Composite materials involve two or more combined components on a macroscopic scale that are insoluble. One of the components is named the "reinforcing

phase," and the embedded constituent is the "matrix." The reinforcing phase may involve fibers, flakes, or particles, while continuous materials are used as the matrix phase. One of the most significant developments in materials research is the creation of composite materials and production methods [5].

Composite tubes are manufactured in different structures like circular tubes, square tubes, and elliptical cross-section tubes. The most common and studied type is the circular cross-section tubes due to their easy manufacture [6]. Many studies have been attempted to investigate the failure mechanism of composite tubes. Mamalis et al. proposed a theoretical model to predict the crushing loads and absorbed energy in axial collapse. The model was verified experimentally for different geometrical fiberglass composite tubes. Theoretical and experimental results indicate that circular tubes are more efficient in energy absorption [7]. Hu et al. studied the absorption capabilities and features of woven glass cloth/epoxy composite tubes considering the distinct orientation of the fiber. The study showed that fiber orientation affects energy absorption performance significantly [8].

Another research performed by Abosbaia et al. used the wet winding process to fabricate composite utilizing glass, carbon, and cotton with epoxy. The performance of the fabricated segmented when axial force was compared to lateral crushing, composite tubes performed better. Also, the study indicates that improvements in segmented and non-segmented carbon/epoxy composite tubes were insignificant in axial loading. Nevertheless, carbon/epoxy composite tubes had the maximum energy absorption among other segmented composite tubes, including the cotton and glass epoxy composite. Moreover, the performance of segmented cotton-cotton-

carbon/epoxy composites was enhanced by 17%. In contrast, the cotton-cotton-glass/epoxy composites reduced energy absorption compared to the cotton-cotton-cotton/epoxy segmented composites [9][10].

Mahdi et al. investigated the effect of using hybridized carbon/glass sequence composites on energy absorption performance. The study showed reinforcement sequence affects the crushing behavior of the hybrid composites. The glass-carbon-glass (GCG) composites exhibited the best energy absorption among other combinations (i.e., glass-glass-carbon and carbon-glass-glass). This finding is mainly because the interface of the GCG composite is adequate compared to other reinforcements (i.e., CGG and GGC). For example, the carbon layer bent, and glass fiber layers failed in GCG, while GGC and CGG composites failed due to fracture of the carbon layer and debonded glass fiber layers [11].

Polymers are generally used as matrix materials, and they are classified into thermosets and thermoplastics. Epoxy, phenolic, and polyester resins are the most utilized thermosets matrices, while polypropylene, polyvinyl chloride, and polyethylene are the most common thermoplastics settings, as shown in Figure 1 [12]. In addition, due to their high specific strength, and modulus, glass-fiber reinforced plastic (GFRP) and other synthetic fiber-reinforced materials are commonly utilized in crashworthiness research and industry [13, 14].

Many research works have been conducted using glass-fiber reinforced plastic composites to study the crashworthiness of manufactured composite tubes. Nonetheless, there is still necessary to explore the GFRP composite tubes focusing on

the manufacturing procedures that may significantly impact the energy absorption performance. In addition, even though many studies have explored the effect of changing composite tubes geometries, fewer studies have focused on enhancing the commonly used geometries considering changes to the manufacturing process.

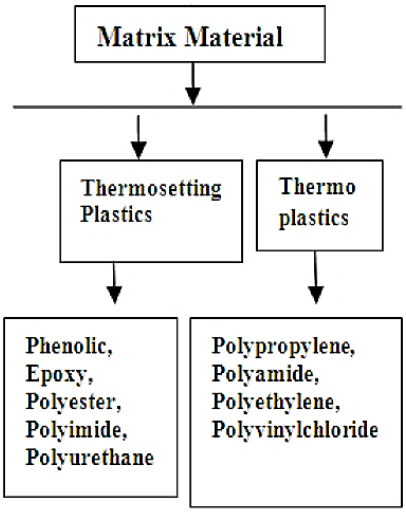

Figure 1. Classification of matrix materials [12].

This research highlights utilizing the conventionally used glass-fiber-reinforced plastics composite tubes (GFRP) while incorporating some changes into the design to enhance crashworthiness. The utilized composite tubes consist of epoxy resin as the matrix material and glass fiber as the reinforcement material. In general, this research aims to look at the effect of changing fiber orientation on the crashworthiness of conventional cylindrical composite tubes. The two main fiber orientation changes include changes introduced to the overwrapping using a winding machine and inner wrapping. Also, this research examines the effect of introducing grooving into cylindrical GFRP composite tubes on crashworthiness performance. The best design of utilized composite tubes and proposed fiber orientation changes are determined by the end of this study.

1.2. Research Objectives

The aims of this research are as follows:

1- To examine the changes in the crashworthiness under quasi-static axial crushing due to overwrapping of cylindrical PVC tubes using specific fiber orientation for GFRP ($\theta = \pm 45^{\circ}$).

2- To examine the grooving impact on crashworthiness of GFRP composite tubes during the quasi-static axial crushing.

3- To study the effect of inner wrapping of the GFRP composite tubes using a specific fiber orientation ($\theta = 90^{\circ}$) on crashworthiness under quasi-static axial crushing.

4- To assess the difference in crashworthiness characteristics between overwrapped composite tubes and composite tubes with overwrapping and inner wrapping subjected to quasi-static axial crushing.

1.3. Significance of the Research

This research sheds light on the impact of modifying the conventional commonly used cylindrical PVC tubes reinforced by glass fiber using specific fiber orientation on crashworthiness characteristics. Also, the effect of grooving the PVC tubes before the wrapping by glass fibers is studied in this project. Besides that, the idea of inner wrapping the PVC tubes were developed in this research to understand its effect on crashworthiness during a quasi-static axial crushing. By the end of this study, the optimal design of PVC tubes considering the investigated modifications is determined.

Composite materials are widely used in the automobile industry, ships, aircraft, space, and wind turbine applications to enhance crashworthiness characteristics and reduce fuel consumption. Accordingly, increasing attention has been paid to utilizing and studying composite materials. This attention is mainly due to their various characteristics over metallic materials, such as being environmentally friendly and lightweight. Also, they have outstanding mechanical features, such as high strength and stiffness and low density, and they have a strong potential for controlling vibration and noise. Most importantly, composite materials exhibit great crashworthiness characteristics, appealing for energy absorption applications [14].

Crashworthiness is a significant design factor that helps maintain and protect passengers' lives during catastrophic crash incidents. The key factor in ensuring the safety of the people in compartments during an incident is to use manufacturing materials with substantial capability to absorb energy without failure. According to statistics, vehicle incidents are one of the top causes of death globally. Therefore, the energy absorption should occur gradually and stably to protect the lives of passengers during a crash. Nowadays, researchers and engineers face the challenge of using composite materials for manufacturing vehicles with high energy absorption capabilities while maintaining an economically feasible design.

1.4. Thesis Layout

This thesis will include five different chapters. Chapter 2 will contain past valuable studies and information about different materials and tubes, several procedures for testing, different capabilities to absorb energy, grooving behavior, and various composite materials' failure mechanisms. Chapter 3 will include a comprehensive

explanation of the methodology used in this thesis. Experiments results with discussion and analysis will be carried out in chapter 4. Lastly, chapter 5 will present the findings of this thesis.

CHAPTER 2: LITERATURE REVIEW

This chapter provides details for different fundamental terminologies used in this research and some relevant reviews about similar work in the literature. In addition, information is provided for composite materials, composites of fiber-reinforced material, matrix materials, composites fabrication process, grooving, quasi-static testing, performance indicators for quantitative energy absorption, composite failure modes, and energy absorption mechanisms, and existing studies on composite tubes' energy absorption.

2.1. Composite Materials

A composite material is characterized by combining two or more different materials with a finite interface between them. The resultant composite material has better properties than the individual constituents. One of the constituents is called the reinforcing phase, which exists in fibers, particles, or platelets, and the other is the matrix phase. Each constituent's chemical, physical, and mechanical properties are conserved, opposing metal alloys. The reinforcing phase typically consists of glass, aramid, or carbon, while matrices include ceramics, metals, or polymers [15]. The reinforcing phase provides the composite material with stiffness and strength while the matrix phase binds the reinforcements, helps distribute mechanical loads and shapes the composite material.

Selecting constituents helps attain the required properties and optimize the properties as per design requirements. In general, composite materials have higher modulus to weight ratios and higher strength than typical materials. This finding helps reduce the system’s weight by about 20-30%, enhancing performance, saving energy,

and lowering environmental impact. Moreover, composite materials enhanced properties may also involve improved chemical and corrosion resistance and low maintenance cost, which extended the life of designed parts. Composites properties greatly impact different industries, including the marine industry, sporting goods industry, and aerospace and military markets. As the understanding of composites grows, more opportunities and development will occur in different industries [16]. Figure 2 shows a general classification of composite materials [17].

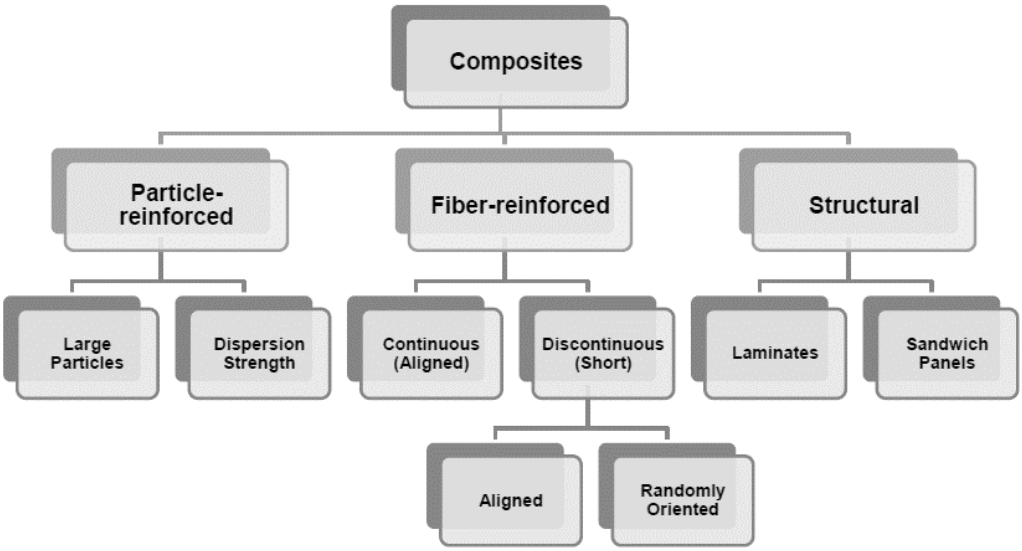

Figure 2. Hierarchy chart of different composite materials classifications [18]

2.2. Composites of Fiber-Reinforced Material

Fiber-reinforced composite materials have higher strength-to-weight and modulus-to-weight ratios than metallic materials [18]. As a result, the demand for natural and synthetic fiber-reinforced composites increased significantly during the past decades. This fact can be attributed to the advantages of FRCs, including the lightweight, high durability, resistance to corrosion, wear, moisture, chemicals, fire, and energy absorption. These properties are favored in several applications involving aerospace, automobile, sports, marine, constructions, etc. In addition, the outstanding

performance of the FRCs makes them a promising alternative to metals and alloys in different industries [19].

In a composite material, fibers are held by matrix resin. The properties of the composite materials, including the strength and stiffness, depend primarily on fiber reinforcement type. Different fibers are available, including glass fibers, carbon "sometimes called graphite" fibers, aramid fibers, boron fibers, quartz fibers, and ceramic fibers. Fibers typically show much higher strength than the bulk form of the material. The strength of the fiber depends on the probability of flaw per unit length, which relies on material volume. As fibers have a lower volume per unit length than the same bulk materials, fibers have higher strength. Table 1 indicates the commercially significant characteristics of certain high-strength fibers [20].

Table 1. Characteristics of Certain High-Strength Fibers Commercially Significant [21]

Type of fiber	Tensile strength, ksi	Tensile modulus, msi	Elongation at failure, %	Density, g/cm³	Coefficient of thermal expansion, 10^{-6} °C	Fiber diameter, µm
Glass						
E-glass	500	10.0	4.7	2.58	4.9–6.0	5–20
S-2 glass	650	12.6	5.6	2.48	2.9	5–10
Quartz	490	10.0	5.0	2.15	0.5	9
Organic						
Kevlar 29	525	12.0	4.0	1.44	–2.0	12
Kevlar 49	550	19.0	2.8	1.44	–2.0	12
Kevlar 149	500	27.0	2.0	1.47	–2.0	12
Spectra 1000	450	25.0	0.7	0.97	…	27
PAN-based carbon						
Standard modulus	500–700	32–35	1.5–2.2	1.80	–0.4	6–8
Intermediate modulus	600–900	40–43	1.3–2.0	1.80	–0.6	5–6
High modulus	600–80	50–65	0.7–1.0	1.90	–0.75	5–8
Pitch-based carbon						
Low modulus	200–450	25–35	0.9	1.9	…	11
High modulus	275–400	55–90	0.5	2.0	–0.9	11
Ultra-high modulus	350	100–140	0.3	2.2	–1.6	10

2.2.1. Glass Fibers

Glass fiber's stiffness is lower than other reinforcements. Still, they are widely used in commercial composite applications due to their relatively low cost, high strength and high impact resistance, and good chemical resistance [21][22]. Thus, one of the main advantages of glass fibers is the high performance per cost ratio. This advantage makes glass fiber the most commonly used reinforcement in composite applications to replace heavy metals. Glass fibers are often used for thermal and electrical insulation due to their poor thermal and electrical conductivity [23][24]. As a result of glass fiber advantages, the global consumption of glass fiber was about 2.6 million tons, increasing exponentially [22].

Different types of glass fibers are available, manufactured by changing raw materials proportions. The main component of glass fiber is silica, and the percent of oxides, i.e., Al_2O_3, B_2O_3, CaO, determines the final glass fiber properties. E-glass and S-glass (also called HT glass) fibers are the most popular forms of glass fibers. E-glass fibers are the first and most commonly used synthetic reinforcement, and they are used when strength and electrical resistivity are required [25]. The S-glass fibers were initially developed and utilized for military applications such as military aircraft components. Then another form called S-2 glass was fabricated and used for commercial applications as it has lower cost and comparable performance. Glass fibers are utilized due to their high tensile strength. S-glass fibers exhibit higher strength, stiffness, and resistance to creep and fatigue [26]. E-glass and S-glass fiber tensile strength can reach 3.4 and 4.5 GPa, respectively. On the other hand, glass fibers have

relatively low tensile modulus and high density so they may be unsuitable for some lightweight structures' applications due to the later drawback.

Table 2 summarizes some commercial glass fibers' physical properties [22].

Table 2. Physical Properties of Some Commercial Glass Fibers [23]

	A-Glass	C-Glass	D-Glass	E-Glass	ECR-Glass	AR-Glass	R-Glass	S-2-Glass
Density (g/cm^3)	2.44	2.52	2.11–2.14	2.58	2.72	2.70	2.54	2.46
Tensile strength (MPa)	3310	3310	2415	3445	3445	3241	4135	4890
Tensile modulus (GPa)	68.9	68.9	51.7	72.3	80.3	73.1	85.5	86.9
Elongation (%)	4.8	4.8	4.6	4.8	4.8	4.4	4.8	5.7

2.3. Matrix Materials

Composite materials consist of fibers and matrix material. As the fibers provide stiffness and strength, the matrix material is important [27]. Matrix material plays a crucial role in determining overall mechanical characteristics considering fibers binding and load distribution [28]. Moreover, matrix material prevents crack propagation as it separates the fibers and helps prevent fiber buckling during compression. Essential requirements of matrix material include infiltration within fibers, not undergoing a chemical reaction, or causing damages to fibers. Composite materials are classified into three main categories according to the type of material matrix. These are the polymer matrix composite (PMC), ceramic matrix composite (CMC), and the metal matrix composite (MMC) with PMC as the most common composites [28][29]. The PMC is characterized by its good properties at room

temperature, light weight, low cost, and ease of manufacturing [29]. Polymer composites are classified into thermoplastics and thermosetting resins [30][31].

2.3.1. Epoxy Resins

Epoxy resins are compounds that involve one or two epoxy groups named epoxide or oxirane. Figure 3 shows the epoxide group, which includes a tight C-O-C ring, and it may exist within the epoxy resin molecule or as a terminal group [32][33][34]. The three-membered epoxide ring can react with different reactants in different ways, giving a versatile range of epoxy resins [35]. Epoxy resins must be cured or cross-linked by polymerization to transfer them into useful products. The epoxy ring is highly reactive with various substances, especially with proton donors, schematically shown in Figure 4. Epoxy resins exhibit lower curing shrinkage than other thermosetting plastics because they are formed by rearrangement polymerization (i.e., chain extension and cross-linking without eliminating small molecules like water). Due to their low shrinkage and ease of fabrication, epoxy resins are well suited for tooling applications such as jigs, and metal shaping molds [36].

Two types of reactions are utilized for epoxy resins, including the direct coupling by catalytic homo-polymerization and reaction with co-reactants called hardeners [35]. Lewis acids or tertiary amines can be used for catalytic polymerization, which typically utilizes a very low concentration of catalysts (<1% of resin's weight) [37]. Many co-reactants can be used, such as polyfunctional amines, acids, acids, anhydrides, phenols, alcohols, and thiols. Safety precautions, including using gloves, wearing face shields, working in a well-ventilated environment (i.e., fume hoods), and developing monitoring policies, must be considered when handling epoxy resins. Epoxy resins may cause skin irritation and asthma-like conditions [32].

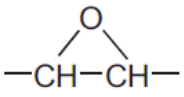

Figure 3. Epoxide ring [33]

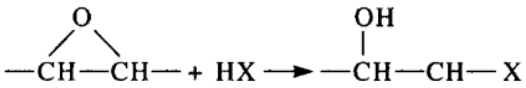

Figure 4. The schematic figure for epoxy ring reaction with a proton donor [33]

The commercial interest in epoxy resins was started by patents developed by Dr. Greenlee from the United States and Dr. Castan from Switzerland [33] [36]. Soon after, epoxy resins were used widely due to their superiority over available thermosets as they pose good thermal performance and their chemical and temperature resistance and strength [36].

Figure 5 indicates that epoxy resins are widely utilized in different applications, including paint and coating, electrical industry, and composite materials, accounting for about 10% of the market. It is expected to increase [36]. Epoxy resins may also be used for wind energy, construction, and adhesives. In addition, epoxy resins yield composite materials characterized by the best properties of most thermosets when combined with fibers (i.e., aramid fibers, glass, carbon) which make them appealing for this area [36].

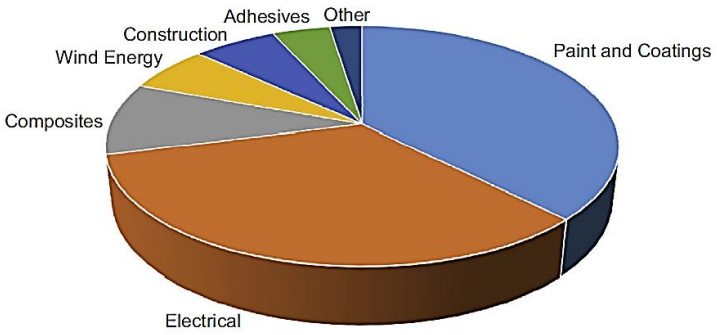

Figure 5: Epoxy resins consumption by world markets [37]

2.4. Composites Fabrication Process

Composite materials can be manufactured using different processes. The selection of the process depends on different parameters such as material, design, and application. Epoxy resins can be utilized as the matrix phase for the composite materials [34]. Utilizing epoxy resins to produce composites can be done through several processes classified into "wet resin" and "prepreg" processes. Table 3 shows some of the processes for composites production using epoxy resins and their associated products [36]. "Wet resin" processes directly depend on combining the epoxy and the fibers, which can be achieved by hand. Due to safety and health policies, closed mold processes such as vacuum infusion and resin transfer molding are favored over epoxy resin open environment processing. Resin transfer molding utilizes a driving force such as pressure or vacuum to flow the resin into a reinforcement placed within a two-sided composite mold. In contrast, the resin infusion uses a one-sided mold which makes it relatively more cost-effective [36].

Moreover, the infusion process is used for fabricating enormous parts of boats and wind turbine blades. Processes that still include the processing of open liquid require enhanced facilities for vapor extraction. Also, vacuum infusion process has the

ability to distribute the resin evenly without any excessive use of resin and work force. However, the needs of several tools to have a proper control on the infusion pressure consider as a drawback because a decreased flow of resin will result in accumulation of resin at the center part of fibre lay-up [38]. Epoxy resins composites can be utilized for manufacturing boats, wind turbine blades, pipes, pressure vessels, printed circuit boards, and automotive and aerospace applications. Besides that, epoxy composites are used to fix steel structures and pipes, especially for offshore applications, which might be affected by different factors, including corrosion, damage impact, and fatigue.

Table 3. Composite Production Processes Using Epoxy Resins

Process	Type of Product
Wet Resin Processes	
Contact molding (hand laminating)	Boats, surfboards, baths, general purpose moldings
Resin transfer molding	Boats, general purpose moldings
Resin infusion	Boats, wind turbine blades
Filament winding	Pipes and pressure vessels
Prepreg Processes	
Press molding	Printed circuit boards
Vacuum bag oven processing	Automotive composites wind turbine blades
Vacuum bag autoclave processing	Aerospace composites

2.4.1. Filament Winding

The filament winding fabrication process is one of the most common open mold methods to fabricate composite materials. The method is highly automated, continuous, and has the advantage of low material cost and utilizing maximum strength of fibers by using continuous reinforcement [16][39]. This method is widely used for several applications involving corrosion-resistant pipes, cylindrical parts, closed-end structures

such as pressure vessels and tanks, aircraft fuselages, besides other applications, for example, fishing rods and golf club shafts [36][40][41]. Storage vessels fabricated by filament winding are used for gas transport and storage (i.e., natural gas, butane) [36].

Figure 6 shows a schematic of the filament winding process [41]. The first step is to wound a filamentous yarn or tow - which can be wetted in a resin or use pre-impregnated tapes as an alternative – around a mandrel. The second stage involves curing the composites by either heating or exposure to infrared radiation (IR). The heating can be achieved via oven or autoclave. The final stage is removing the mandrel and obtaining the composite [16][41].

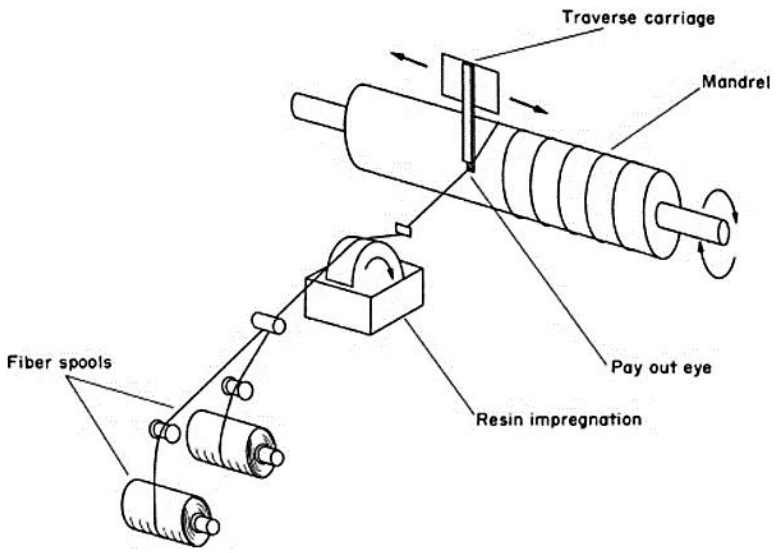

Figure 6. Schematic representation of filament winding process

2.5. Grooving

The properties of thin-walled steel tubes with annular grooves in terms of crashworthiness were investigated by Hosseinipour et al. [42]. One of the most efficient methods of energy absorption is the use of thin-walled tubes collapsing plastically in axial compression. These tubes have several advantages: slight volume and weight,

simple construction, affordability, and stability while crushing. To adjust the buckling mode and estimate the energy absorption capacity of the tubes, circumferential grooves were cut on the tubes alternately internally and externally. The quasi-static axial crushing test findings reveal that the presence of grooves of varying lengths can affect the load-displacement curve and the energy absorbed by the axial crushing of tubes. Grooves may also stabilize deformation behavior; hence the proposed approach could be an excellent choice for a regulated energy absorption element. Compared with the non-groove specimen, the presence of grooves decreased energy absorption. Since a portion of the applied load is dissipated during the creation of the plastic hinges, the remaining load causes bending between the plastic hinges, which results in stretching work. The addition of the groove assists the failure to be directed along the groove trough. Because of this incidence, the effort required for a complete crush was reduced.

2.6. Quasi-static Testing

A quasi-static test will be applied to the samples using a conventional universal testing machine. The machine consists of two parallel plates. First, the model will be fixed between them. Then the upper plate will descend at a constant velocity while the bottom plate is fixed. This process will compress the sample. Usually, the crushing rate in quasi-static testing ranges between 1 mm/s to 11 mm/s. In a real-life collision, the crushing speed of the crashed objects decreases until the objects stop, which is not identical to the quasi-static test situation [43]. However, it is helpful to investigate the behavior of the samples in a quasi-static test to ignore the strain rate dependence and investigate other factors.

On the other hand, in most automobiles, composite tubes are supported at one end by a higher strength structure similar to the quasi-static test. Thus, the tube may

display similar behavior to what is found by the quasi-static test [44]. All in all, the advantages of quasi-static testing are [45]:

a) Due to its slow crushing speed, investigating failure behavior is easier than the impact test, which quickly happens.
b) The quasi-static test equipment has a lower cost than the impact test equipment.
c) The conditions of the test can be easily controlled.

On the other hand, the quasi-static test disadvantage is that it does not perfectly represent real-life crash circumstances.

2.7. Performance Indicators for Quantitative Energy Absorption

Composite materials Energy absorption can be measured quantitatively and qualitatively. The qualitative assessment can determine the composite failure mechanisms, force-displacement properties, and crashing behavior. However, the quantitative assessment gives an idea about the capability of the structure energy absorption since it investigates the crashworthiness characteristics [46]. Below are some critical parameters reflecting the crashworthiness characteristics of a structure. The general outline of the load-displacement curve for the composite is shown in Figure 7, and some necessary quantities to calculate these parameters.

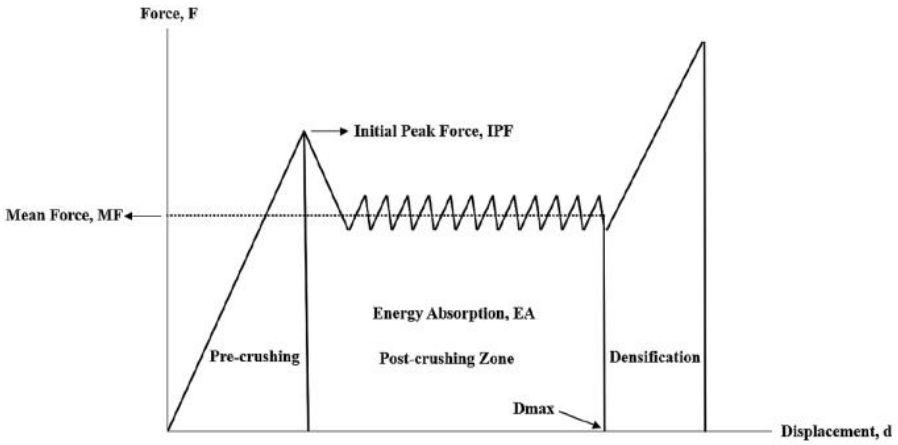

Figure 7. The general form of the load-displacement curve for composite tubes [47]

2.7.1. Initial Peak Force

The plastic deformation of the plastic tube begins only after the initial peak force (IPF) is reached. It is desirable to have a small phase turning point between the IPF and the mean force (MF). Because minor phase turning point means that the structure energy absorption is less affected after the deformation, maximizing the energy absorption and minimizing the reaction force [48].

2.7.2. Energy Absorption and Specific Energy Absorption

The composite structures' ability to absorb energy is described graphically as the area underneath the load-displacement curve. Which can be calculated mathematically by [49]:

$$EA = \int_0^{Dmax} Fds \tag{1}$$

Where F is the compressive load, the energy absorbed per unit mass of the structure is specific energy absorption (SEA).

$$SEA = \frac{EA}{m} \quad (2)$$

The structure mass under compression is given as m.

2.7.3. Mean Crushing Force

The mean crushing force (MF) definition is the mean force experienced by a composite object under axial loading. Mean crushing force is normally calculated without the forces occurring in the densification phase [46]. It can be estimated by

$$MF = \frac{EA}{Dmax} \quad (3)$$

Where $Dmax$ is the composite structure's maximum displacement before the densification stage starts.

2.7.4. Crush Force Efficiency

Crush force efficiency (CFE) represents the relationship between initial peak load and mean force experienced by the composite structure [47]:

$$CFE = \frac{MF}{IPF} \quad (4)$$

The ideal situation for the energy absorption is when the CEF ratio is 1, which means that the structure will continue to sustain the initial peak force value even after crushing, maximizing the energy absorption area [47].

2.7.5. Instantaneous CFE

MF is utilized to calculate other factors like CFE since the post-crushing stage of the structure is widely fluctuating. However, MF and instantaneous force will be the same at some points. Thus, a new variable, "Instantaneous Crush Force Efficiency (iCFE)," was found. The iCFE provides the percentage of the force points equal to or within a specific value to the MF. In this study, the specific value will be ±0.1. It is calculated by dividing the MF on the post-crushing stage instantaneous force values at each displacement.

$$iCFE = \frac{MF}{F_i} \quad \text{post-crushing stage} \tag{5}$$

The results will be plotted against the displacement and compared to the MF. If the ratio between the MF and iCFE is one, that means that at this point, the instantaneous force and the MF are equal. Therefore, these are the best forces for studying crushing behavior. iCFE will be calculated for each tested structure. If the CFE equals one or is very close to it and the high iCFE percentage, the structural failure is extraordinarily stable.

2.8. Composite Failure Modes and Energy Absorption Mechanisms

It is important to understand failure modes of crushed composite structures to anticipate how they would behave [50]. For example, crushing composites by applying quasi-static axial force would result in two: stable and unstable behaviors. The stable failure is when a developing compression load onto the specimen reaches an initial peak. Yet, it would bear that load with a slight deflection and a relatively small drop in the load-bearing capacity. Thus, the stable failure specimen can conquer more energy. In contrast, the load-bearing capacity in an unstable failure would rapidly drop after

reaching the initial peak; hence, no more developing load would be carried.

A key factor in controlling the failure mode of a structure is the dimensions. For example, the length to diameter ratio (L/D) for a cylindrical structure would anticipate the composite's failure mode shown in Figure 8. In addition, the diameter to wall thickness (D/t) and a side length to wall thickness (S/t) would contribute to deciding the failure mode [51].

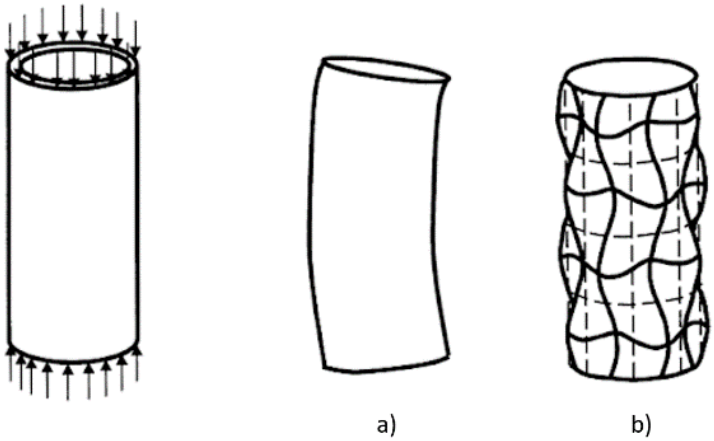

Figure 8. Illustration of failure modes for a cylindrical composite [52]

Figure 8 shows how various dimensions would result in different outcomes from crushing a composite cylinder. A global bulking was found in (a), while in (b) local bulking were found. Hence, suboptimal energy absorption would occur in the global bulking behavior, which is undesired.

The clearest method to observe the failure mode is by applying quasi-static axial compression load to a cylindrical composite tube with a smaller (D/t) ratio [50]. As a result, the failure behavior can be identified as three major modes: Mode-I, Mode-II, and Mode III.

First, Mode-I, it is known that this mode of failure can absorb energy the most among the three modes, hence, the most stable behavior. It can be determined that the tube is undergoing a Mode-I failure by its unique behavior of micro fragments as an axial, long interlaminar, and intra-laminar cracks through the lamination, which can be observed and also extended. In contrast, the crushing load increases; these cracks can be called fronds [53].

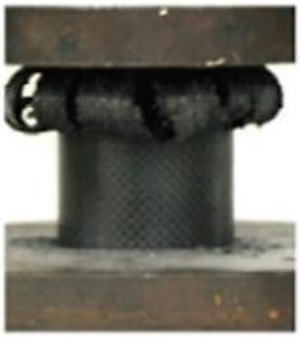

Figure 9. Developing fronds [54]

Thus, and due to the fronds, the composite tube specimen would look like a mushroom during crushing. However, the associated forces with the fronds are compressive in the fronds and the debris wedge. The inner and outer fiber resist the longitudinal crack, resulting in the friction force between the fronds and the crushing plate as the fronds tend to slide on its surface, the friction force between the debris wedge and fronds, and friction force between the fronds and the lamination [55]. These fronds' specifications can vary based on the lamination properties, fiber, and matrix. Therefore, these forces absorb more energy while crushing progress, similar to axial tube splitting [56], [57].

Second, Mode-II is known that it is the least failure mode that can absorb energy among the three modes, hence, the most hazardous behavior. Third, it can be easily

identified as it involves a brittle fracture due to transverse shear. Consequently, a longitudinal or circumferential crack would occur. Subsequently, the fractured fragments would separate or keep a link in some cases.

Figure 10. Mode-II fracture [58]

Progressing crushing load can cause interpenetration of the fractured parts of the specimen, which would develop residual load-bearing capacity. Hence, the friction force in this mode does not have a considerable energy absorption as Mode-I [59]. On the other hand, when the fractured fragments fall from the crushing zone, they will no longer contribute to absorbing energy.

Finally, Mode-III is considered very close to Mode-I in the behavior of the composite when subjecting it to quasi-static axial crushing force and has a relatively moderate ability in absorbing energy. However, repetitive behavior is observed from the composite, folding, and hinging during crushing increasing load. In other words, the load would accumulate and then cause the first hinge and fold in the tube, then when it is enough for the next one, it happens, and so on until the tube fails.

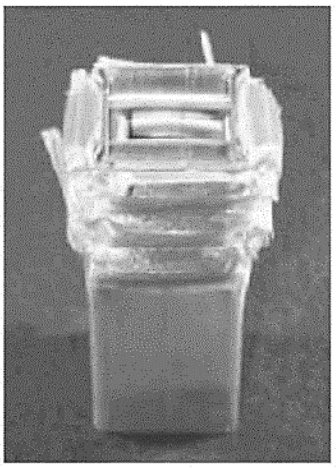

Figure 11. Composite tube undergoing Mode-III failure mode [60]

As the hinges are formulated, the progressive crushing load would cause the composite to have a sizable amount of circumferential and interlaminar fractions [53]. However, comparing this failure mode to Mode-I and Mode-II is that the composite does not damage comprehensively. Thus, it is very useful for the cases where the crushing subject is desired to stay in one piece while energy is absorbed. Therefore, in such cases, the hybrid composites of ductile fibers are introduced to obtain such behavior [61].

2.9. Existing Studies on Composite Tubes' Energy Absorption

In this section, previous research regarding how variating parameters can affect the crashworthiness characteristics of composite tubes while undergoing a crushing load, hence, fiber winding orientation, matrix material, tube geometry, and crushing method.

2.9.1. "Experimental Investigation of the Quasi-Static Axial Crushing Behavior of Filament-Wound CFRP and Aluminum/CFRP Hybrid Tubes."

A study has been conducted to test 25 settings of a composite tube's behavior with contrasting settings and the genuine tube's behavior, undergoing quasi-static axial crushing load. Sun et al. [62] have developed hybrid aluminum tubes (CFRP) with a variation of two parameters: the orientation angle of reinforcing carbon fiber and the wall thickness. Hence, four fiber angles were tested: 25°, 50°, 75°, and 90°, filament-winded, and three wall thicknesses: 3, 6, and 9 layers of reinforced carbon fiber. Therefore, 12 reinforced tubes, 12 CFRP without the tube, and a genuine tube. The reinforced carbon fiber tubes were matrixed by epoxy, and the crushing machine was INSTRON-5985. However, other parameters were set to be a room temperature ambient, 150 kN, and crosshead velocity of 4 mm/min.

Testing a fixed wall thickness for both CFRP with the tube and CFRP without the tube concluded that the increase in the angles decreases the Peak Crushing Load (PCL), which in turn decreases the Energy Absorbed (EA) and the Specific Energy Absorbed (SEA). Testing a fixed winding angle for both CFRP with the tube and CFRP without the tube increased the wall thickness to increase the PCL. Thus, EA and SEA would increase. Testing CFRP with tube and CFRP without tube against genuine tube showed that reinforcing carbon fiber with both conditions increases the overall PCL, EA, and SEA.

To sum up, this study contributed to concluding that variant settings of a composite tube can potentially affect the Peak Crushing Load, EA, and SEA. Thus, the CFRP w/ tube, nine layers, and winding angle of 25° had the maximum SEA value of

79.05 J/g, then the CFRP w/o tube, nine layers, and winding angle of 25° resulted in 48.74 J/g. As a result, this concluded that the energy absorption would increase with the presence of the genuine tube reinforced with composite. Moreover, changing these settings can also affect the failure mode of the CFRP with or without the tube.

2.9.2. "Comparison of Energy Absorption of Carbon/Epoxy and Carbon/PEEK Composite Tubes."

Hamada et al. [63] examined fiber/epoxy against fiber/PEEK tubes to identify the effect of thermoplastic and thermosetting polymers. In addition, unidirectional prepreg fabrics of 0°, ±30°, and ±45° to the tube's axis. Finally, A few composite tubes

Testing an inner tube, using Mand 250 kN servo-hydraulic, that is overwrapped with carbon fiber and using epoxy as the composite tube's matrix material, the carbon fiber used is Q-112/HTA Toho Rayon Co with 55% of prepregs fraction fiber volume. Hence, the crosshead speed for the chamfered specimens was constant at 1 mm/min and 0.01 mm/min for the conventional square end. As a result, the chamfered specimen of 0° winding cracked at a low crushing load parallel to the winding angle. The stable crushing for this configuration of the composite tube was found at the conventional specimen with ±45°. Testing an inner tube, using Mand 250 kN servo-hydraulic, that is overwrapped with carbon fiber and using PEEK as the composite tube's matrix material, the carbon fiber used is APC-2/AS4 ICI-Fiberite Co with 61% of prepregs fraction fiber volume. Hence, the crosshead speed for the chamfered specimens was constant at 1 mm/min and 0.01 mm/min for the conventional square end. The most meaningful result for this configuration of the composite tube with chamfered specimen was 0° winding by SEA value of 180 kJ/kg. Thus, stable crushing behavior was

observed at 0° winding.

It can conclude that the fiber rinsed by PEEK matrix material can resist crack formation. Moreover, increasing the winding angle would decrease the mean crush stress, specific energy absorption, and mean crush load.

2.9.3. "Crushing Response of Composite Corrugated Tubes to Quasi-Static Axial Loading."

This study aimed to examine corrugated tubes to determine the effect of corrugating angle and reinforcing material on the crashworthiness behaviors. Elgalai et al. [64] tested corrugated tubes with corrugating angles (β) of 10°, 20°, 30°, and 40° Figure 12. In addition, two different reinforcing materials were examined; the first was woven roving glass fiber fabricated using the wet roving wrapping method and 0.55 volume fraction fiber. At the same time, the other one was 90° fiber orientation of unidirectional carbon fiber fabricated using filament method of winding with 0.56 volume fraction fiber; hence, epoxy was used as the matrix material for both. However, Instron 8500 digital-testing machine was used to conduct a quasi-static axial crushing load on all the specimens with a maximum capacity of 250 kN and a constant crosshead speed of 25 mm/min.

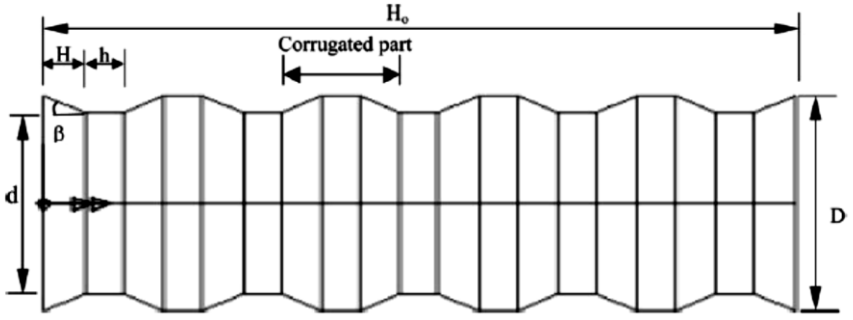

Figure 12. Side view of a corrugated tube [64]

This study had three main results; first, the glass fiber corrugated composite tube showed a better stable load-carrying behavior than the carbon fiber corrugated composite tube. Second, the SEA increased significantly for carbon fiber corrugated tubes as the corrugating angle increased. Finally, there was no clear trait for glass fiber corrugated composite tubes as the corrugating angle increases or decreases against the SEA.

2.9.4. "Crush Responses of Composite Cylinder Under Quasi-Static and Dynamic Loading."

This study aimed to examine a tulip trigger composite tube undergoing an increasing strain rate to understand the energy absorption behavior difference. Hence, Chiu et al. [65] tested such carbon fiber with epoxy matrix composite tubes under dynamic crushing load with different strain rates but not exceeding 100 s^{-1}Against quasi-static crushing load to identify how would that affect the failure mode that could lead to measure the steady-state and peak loads, SEA, and crushing force efficiency, through load-displacement response in post-test behavior.

The tulip-triggered composite tubes that underwent a dynamic crushing load did not change failure mode while the load increased; hence, the steady-state compression load and SEA remained relatively constant. Even though the procedure that has been followed in this study could reveal some changes in the specimens' behavior, such as force efficiency and the peak force, summing up, as the reinforcing fiber's volume fraction increases, the effect of dynamic crushing load can be neglected.

2.9.5. "An Experimental Investigation into Crushing Behavior of Radially Stiffened GFRP Composite Tubes."

The geometric status undergoing a quasi-static axial crushing test is a major factor in the failure behavior and energy absorption capacity. Thus, Mahdi and Sebaey [66] studied four E-glass woven fabrics with an epoxy matrix with different transverse cross-sections to determine the optimum one in the crashworthiness behavior. Hence, one conventional tube and three unusual structures were used, and all of them underwent the same test conditions Figure 13. These four composite tubes were coated with eight plies and crushed under a constant crosshead speed of 15 mm/min.

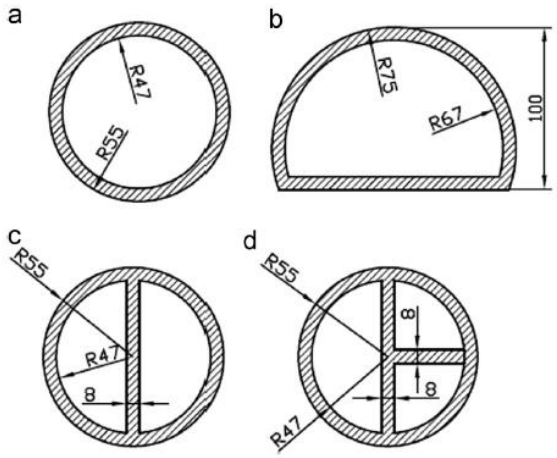

Figure 13. Cross-sectional view of the four used composite tubes (mm) [66]

This study concluded that the crashworthiness characteristics could be modified by fabricating inner geometric support as the optimum cross-section with the highest peak load with 41% enhancement, SEA (38%), EA, crush load efficiency, and average crush load (98%) was (d). In addition, tube (c) results were less efficient, yet, better than the conventional circular tube and tube (b), respectively.

2.10 Summary

This chapter has reviewed the literature related to this thesis. Then, the manufacturing aspects of fibers, matrix, and composites used later are reviewed. Finally, the crashworthiness parameters that affect the collapsible energy absorption has explained in detail.

CHAPTER 3: METHODOLOGY

This chapter describes the methodology used in this thesis. Consequently, the grooving process, outer fabrication of GFRP, inner fabrication of GFRP filament, formation of specimens, testing procedure, and calculations of energy absorption to discuss the results have been explained in detail.

3.1. Grooving Process

In this thesis, the grooving process is meant for cutting some material in a specific pattern along the whole tube. These grooves were fabricated using a CNC machine coded to cut the required material with the required pattern. This method is not applied to all the specimens, which will help investigate the difference between the groove-less tube and the grooved tubes by studying the features of absorption energy of longitudinally circular tubes underneath the axial load. Both tubes will be reinforced externally and some internally with a specific type of glass fiber. Figure 14 shows a schematic of the circular grooved tube fabricated with the dimensions proposed.

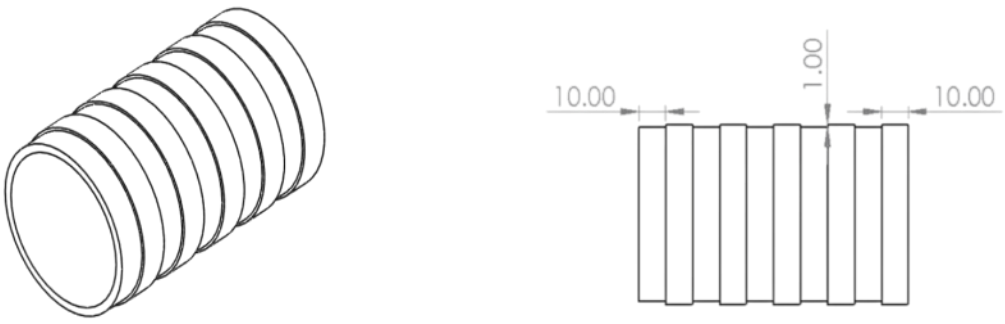

(a) (b)

Figure 14. (a) Isometric view of the grooved tube, (b) Grooving dimensions in mm.

3.2. External Fabrication Process

The winding method is an automated open molding technique that employs a rotating mandrel as the mold to fabricate the glass fibers over PVC pipes. It provides a high tensile strength that results from a high degree of fiber loading. The fiber fabrics were supplied continuously through a resin bath to glue the fibers over the PVC. For this thesis, composite tube specimens were fabricated from PVC as the main pipe, E-type glass fibers as reinforcing material, and epoxy resin as a matrix material. The hardener-to-epoxy resin ratio is 30 parts of hardener to 100 parts epoxy resin. The roving feed is routed through a trolley that travels along the mandrel's length. The reinforcement was installed in a preprogrammed geometric arrangement that gives optimal strength in the required directions. The reinforced PVC pipe was removed after applying the required number of fiber layers, eight layers of glass fiber, for reinforcing. The winding angle used in this thesis for all specimens is ± 45^{o}, as angles are not an interesting part of this study. The longitudinal axis of the pipes corresponds to the reference axis with an angle of 0^{o}. In this thesis, all the grooved and non-grooved tubes will be reinforced externally with the same amount of glass fibers, unlike the internal fabrication, to study the other effects and the overall effect of external reinforcing. Table 4 shows the parameters of the 5-axis filament winding machine used to reinforce the PVC tubes with glass fiber. Also, externally reinforced tubes with glass fiber will be shown in Figure 15.

Table 4. Overview of the Fabrication Process Winding Variables

Fiber speed (m/min)	Spindle speed (RPM)	Feed (m/min)	Winding angle (degree)
25	27	10.6	± 45

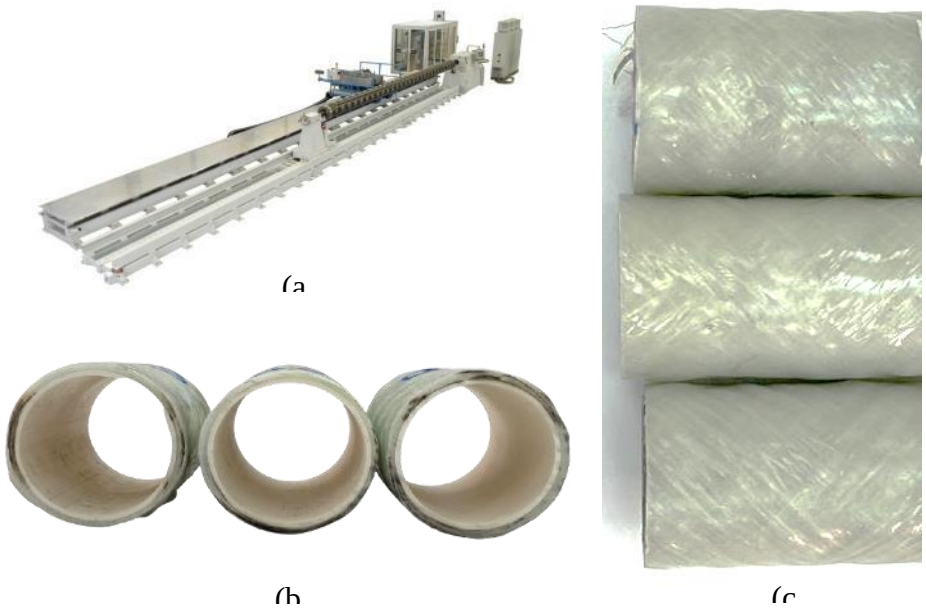

Figure 15. a) 5-axis machine of filament winding, (b&c) ± 45^{o} externally winded tubes

3.3. Inner Fabrication Process

The inner winding fabrication method is similar to the external winding method explained before. Also, epoxy resin will be used as a matrix material to glue the fibers to the tube. The inner winding process will be done manually. Bicycle tubes will be filled with air but not reach maximum capacity. Then, the tubes will be coated with wax. The wax will play the role of the insulation layer between the bicycle tube and the epoxy resin to be able to remove the bicycle tube later. After that, four layers of fiber woven fabric will be wrapped around the waxed tube, and epoxy resin will be applied during wrapping. Finally, the PVC tube will be inserted above the fiber woven fabric with epoxy resin, and the bicycle tube will be filled maximally with air. This method will not be applied to all the specimens. Accordingly, some will be grooved, and some not study the effect of inner wrapping on the crashworthiness of reinforced pipes.

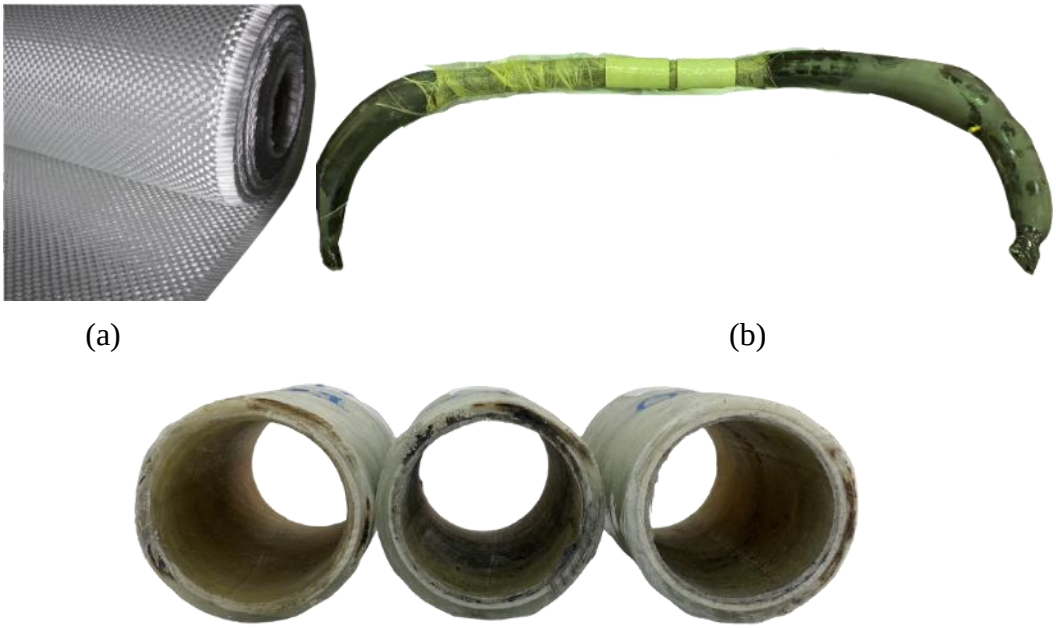

Figure 16. (a) Glass fiber fabric, (b) Inner wrapping process, (c) Internally and externally wrapped tubes

3.4. Loading Conditions

The INSTRON material testing equipment was used to perform quasi-static crushing. Before the testing began, both bottom and top plates were positioned to locate with contact on the surfaces of the tested specimens. The testing machine's bottom plate remained static as a stationary base, but the top plate slid downwards steadily. The crushing speed for all specimens was 50 mm/min and reached a displacement around 85 mm. Although, most of the tested specimens experienced material densification over a displacement around 75 mm. Figure 17 below will demonstrate the testing loading condition used in this thesis.

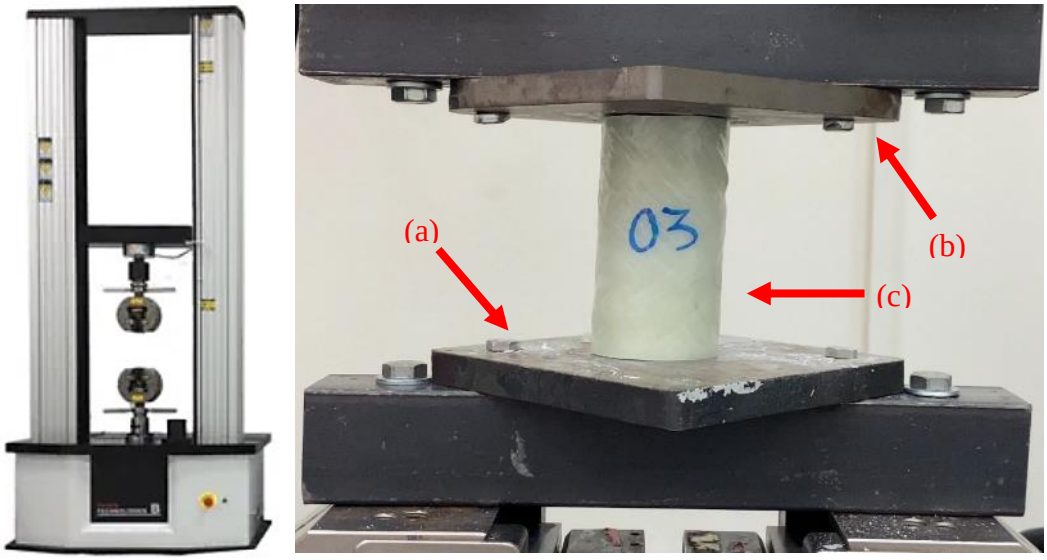

Figure 17. INSTRON testing machine, (a) Bottom plate, (b) Top plate, (c) Tested specimen

3.5 Experimental Samples Procedure

In this section, preparing the tested specimens will be explained in detail to clear the idea of the comparison in this thesis. As explained before, the specimens are divided into two main categories depending on the grooving. Inside each category, there are two different types of tubes depending on the wrapping of the glass fiber, if it is externally only or internally. In the end, PVC will play the role of control samples since it is a well-known sample to assure analyses are appropriately performed so that results are reliable. A hierarchy chart explains the sample tested in Figure 18.

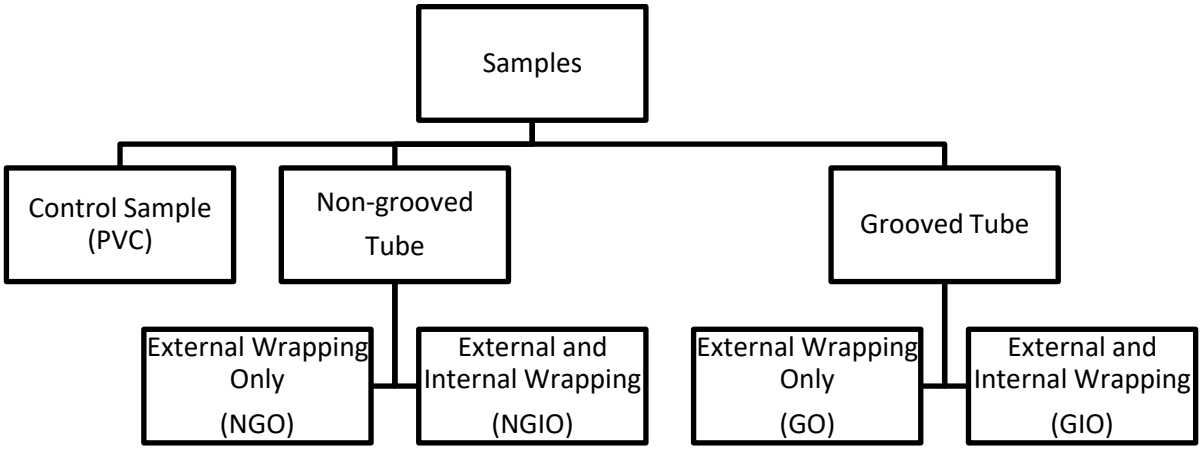

Figure 18. Hierarchy chart of the tested samples

PVC specimens were cut directly from the pipe for control samples since there is no wrapping required at this stage. The samples length was 100 mm approximately. Then, a file tool was used to smoothen the edges of the tubes to ensure the faces were flat and perpendicular to each other. The final average length for the control samples was 97 mm. The PVC pipe itself has a 50 mm outer diameter and 46 mm inner diameter, which means the thickness of the tube is 2 mm. Figure 19 below shows the dimension for the control sample in mm.

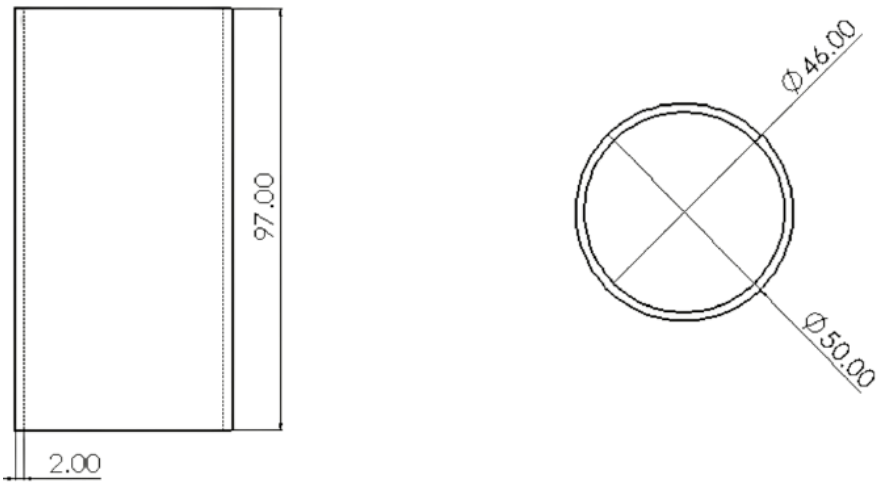

Figure 19. PVC sample dimensions

The first sample category in this thesis uses a non-grooved tube with the same dimension as the control samples. As explained in the hierarchy diagram, the samples were divided into two sub-categories in this category. First, an ordinary PVC pipe fixed on the 5-axis machine to be overwrapped externally with eight layers of glass fiber as described earlier. After wrapping the PVC pipe, it had been cut for small samples with 100 mm length each. Then, after smoothening the edges, some of the samples were taken to be wrapped internally with four layers of glass fibers, and the others were kept as they are. Figure 20 shows the dimensions in mm for all the samples wrapped externally only.

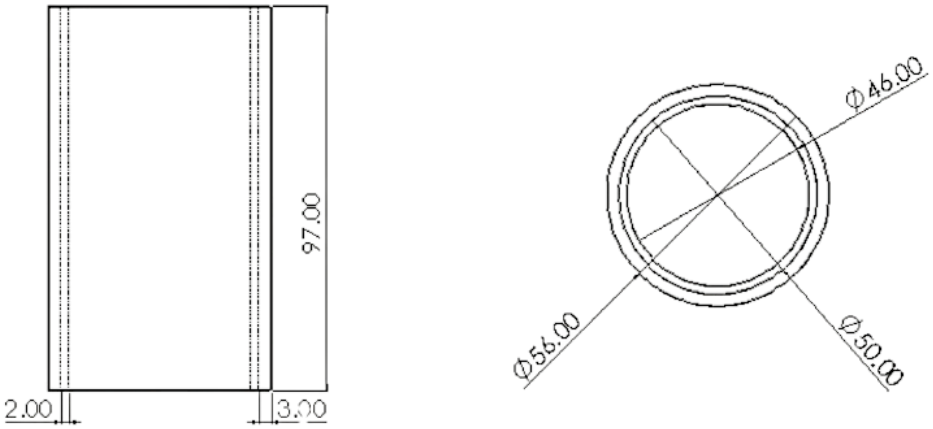

Figure 20. NGO sample dimensions

The outer diameter of the external wrapped samples was 56 mm approximately. So, the thickness of 8 layers of fiberglass is 3 mm almost. Alternatively, the dimensions of the samples with inner wrapping will be shown in Figure 21 below—all dimensions in mm.

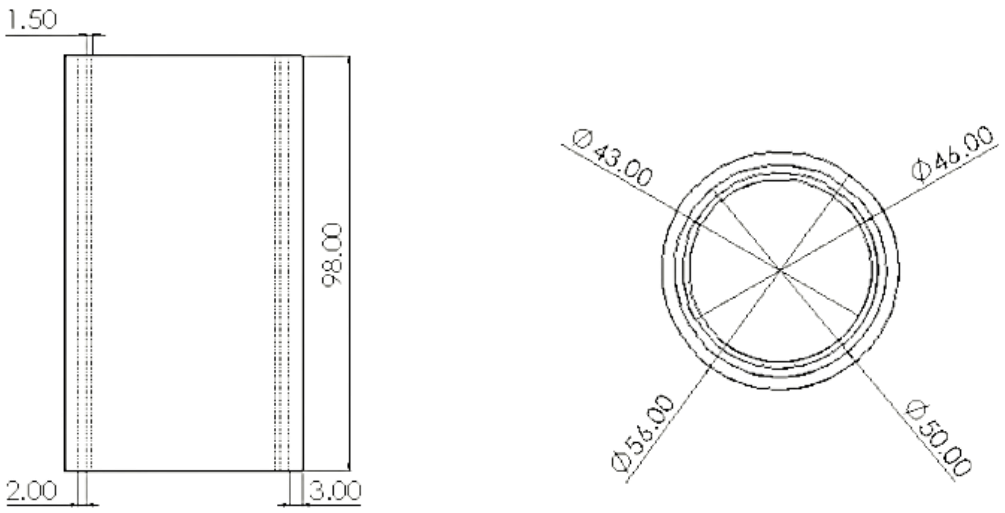

Figure 21. NGIO sample dimensions

The inner diameter of the internally wrapped samples was 43 mm approximately. So, compared with the original inner diameter of the tube, the thickness of the four layers of fiberglass that wrapped inside is around 1.5 mm.

The second sample category in this thesis uses a grooved tube with the same dimension as the control samples. As explained in the hierarchy diagram, the samples were divided into two sub-categories in this category. First, an ordinary PVC pipe is fixed inside the CNC machine and coded to cut a 1 mm required grooves in a pattern that leaves 10 mm between each groove. Then, the same method of non-grooved tube followed and divided into two sub-categories as the non-grooved tube. Figure 22 shows the dimensions in mm for all the samples wrapped externally only.

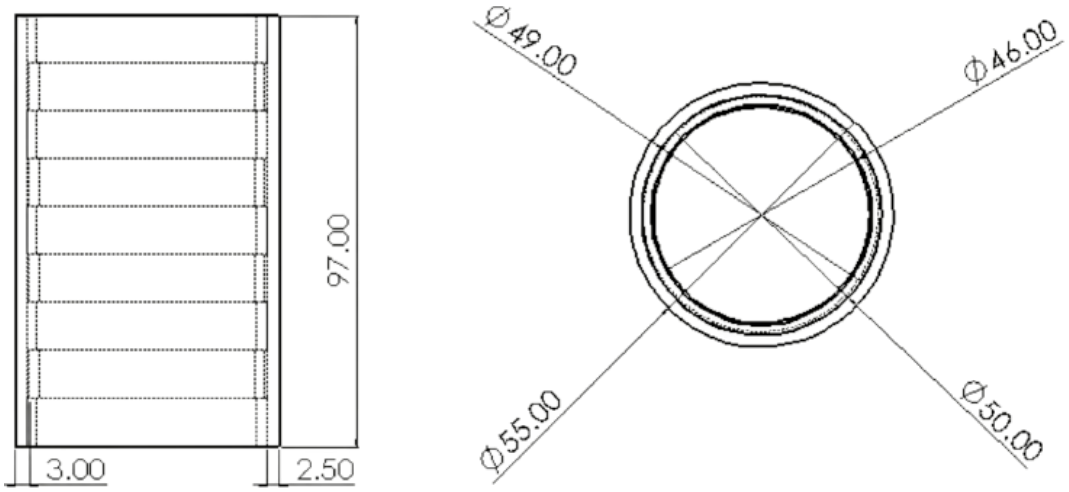

Figure 22. GO sample dimensions

The outer diameter of the external wrapped samples was approximately 55 mm, but the PVC tube's outer diameter was 50 or 49 mm due to the 1 mm groove. So, the thickness of 8 layers of fiberglass is 3 mm almost. Alternatively, the dimensions of the samples with inner wrapping will be shown in Figure 23 below—all dimensions in mm.

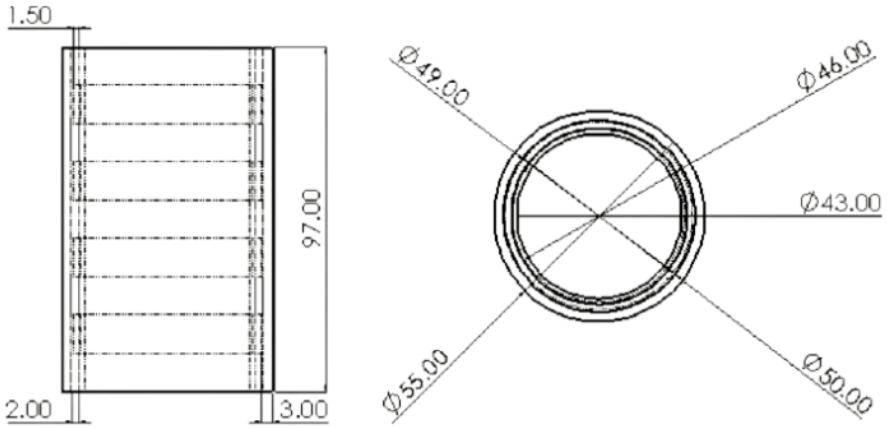

Figure 23. GIO sample dimensions

The inner diameter of the internally wrapped samples was 43 mm approximately. So, compared with the original inner diameter of the tube, the thickness of the four layers of fiberglass that wrapped inside is around 1.5 mm.

A total of three tests were performed as a standard for each of the four different wrappings or grooving styles. It is worth mentioning that three tests were also performed on PVC pipe samples of the same size that were not wrapped to verify the results obtained and serve as control samples for demonstrating the efficacy of the glass fiber/epoxy reinforcement or the grooving. Because the masses of the samples were needed for particular energy absorption calculations, they were all weighed before the compressive testing.

Moreover, a computational online search engine was used for axial loading tests to calculate the area under the load-displacement curves to calculate the energy absorption. Before that, the curves were divided into three stages, pre-crush, post-crush, and material densification stages, as shown in Figure 24 below.

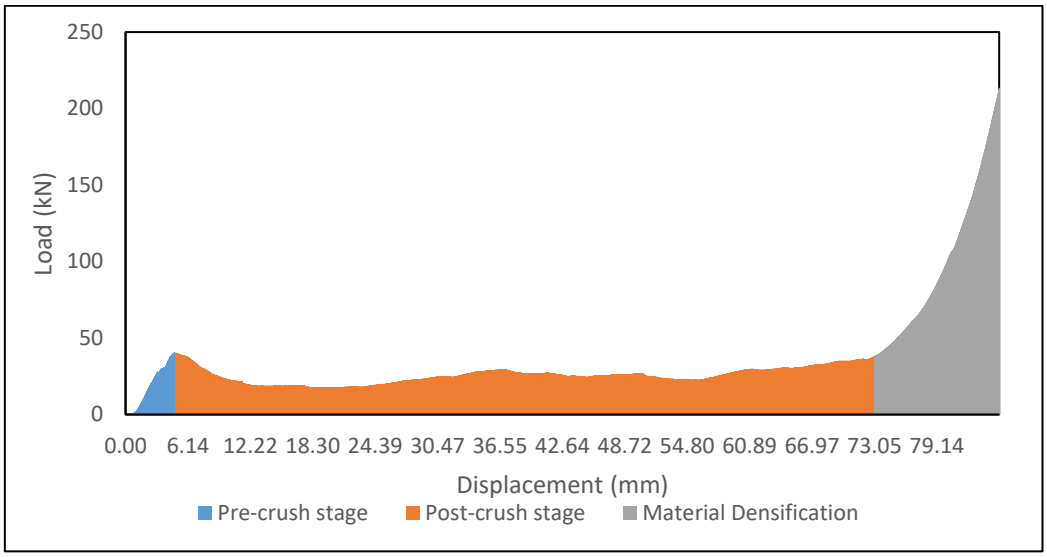

Figure 24. load-bearing graph showing the three stages for a random sample

After dividing the load-displacement graph into three different stages, MS Excel was used to create the trendline for each stage and the corresponding equations for each stage. Then, these equations were integrated using a computational online search engine to find the area under the curves.

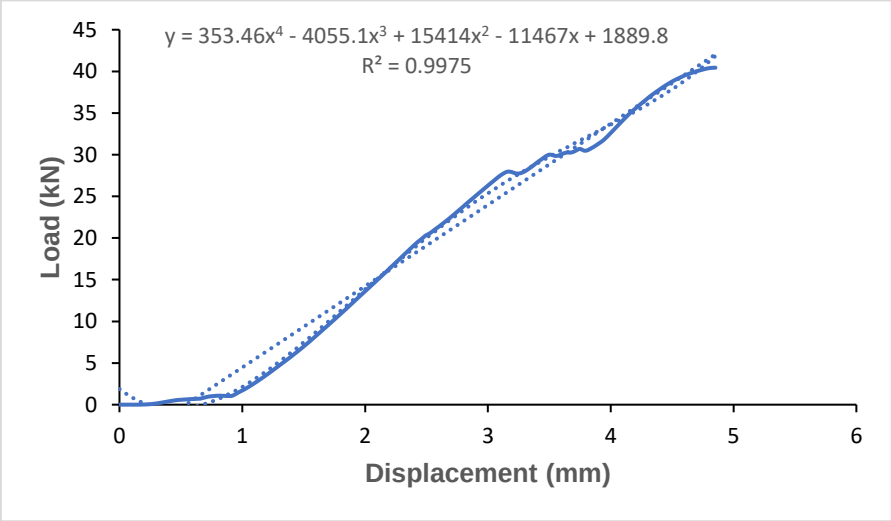

Figure 25. Pre-crushing stage with required trendline and equation

The graph above shows a high R2 value, proving that the trendline is a decent fit for the used data. Also, it is noted that R^2 values for all the trendlines were above 0.91. These graphs will be implemented to calculate the energy absorption for the average load-displacement values of the three tests carried out for each specimen. Also, a manual method was used to double-check the integration by calculating the area under the curve using the midpoint Riemann sum formula.

3.6 Discussion

This chapter has focused on the methods and stages implemented to carry out the present study. Discussing these methods in detail is essential for understanding the experimental work to examine the effect of grooving, external, and internal GFRP overwrapped PVC tubes on crashworthiness characteristics.

CHAPTER 4: RESULTS AND DISCUSSION

This section will carry out the findings of the quasi-static compression test on the various composite specimen tubes, and the results of each specimen will be presented and discussed. In the beginning, the results of reinforcing PVC tubes with GFRP will be demonstrated specifically for each specimen category, the effect of outer wrapping, inner wrapping, and the effect of grooving also. The effect of several factors will also be presented, examined, and compared in detail, such as the behavior of load-bearing, the capability to absorb energy, and crush force efficiency and followed by a sample configuration to select the overall best performance sample.

4.1. Effect on Load Bearing Behavior

This thesis studied the effect of using the GFRP to reinforce the PVC in several aspects. So, to distinguish these effects, it is necessary to study first the behavior of a PVC tube according to the load-bearing behavior to build the comparison of other implemented tubes. The results of each specimen tube will be presented individually. Then, the non-grooved tubes will be compared alone and the grooved also to see the effect of inner and outer wrapping of GFRP on the load-bearing behavior. Finally, a comparison between the grooved and non-grooved tubes has been performed to show the effect of the grooves on load-bearing behavior. All specimens will be represented in the load-displacement curve and some images representing the axial compression test stages. That will be applied to the PVC control sample also. Starting with the PVC specimen as the control sample, Figure 26 shows the compression process as the test images and the load-displacement curve for the PVC tube.

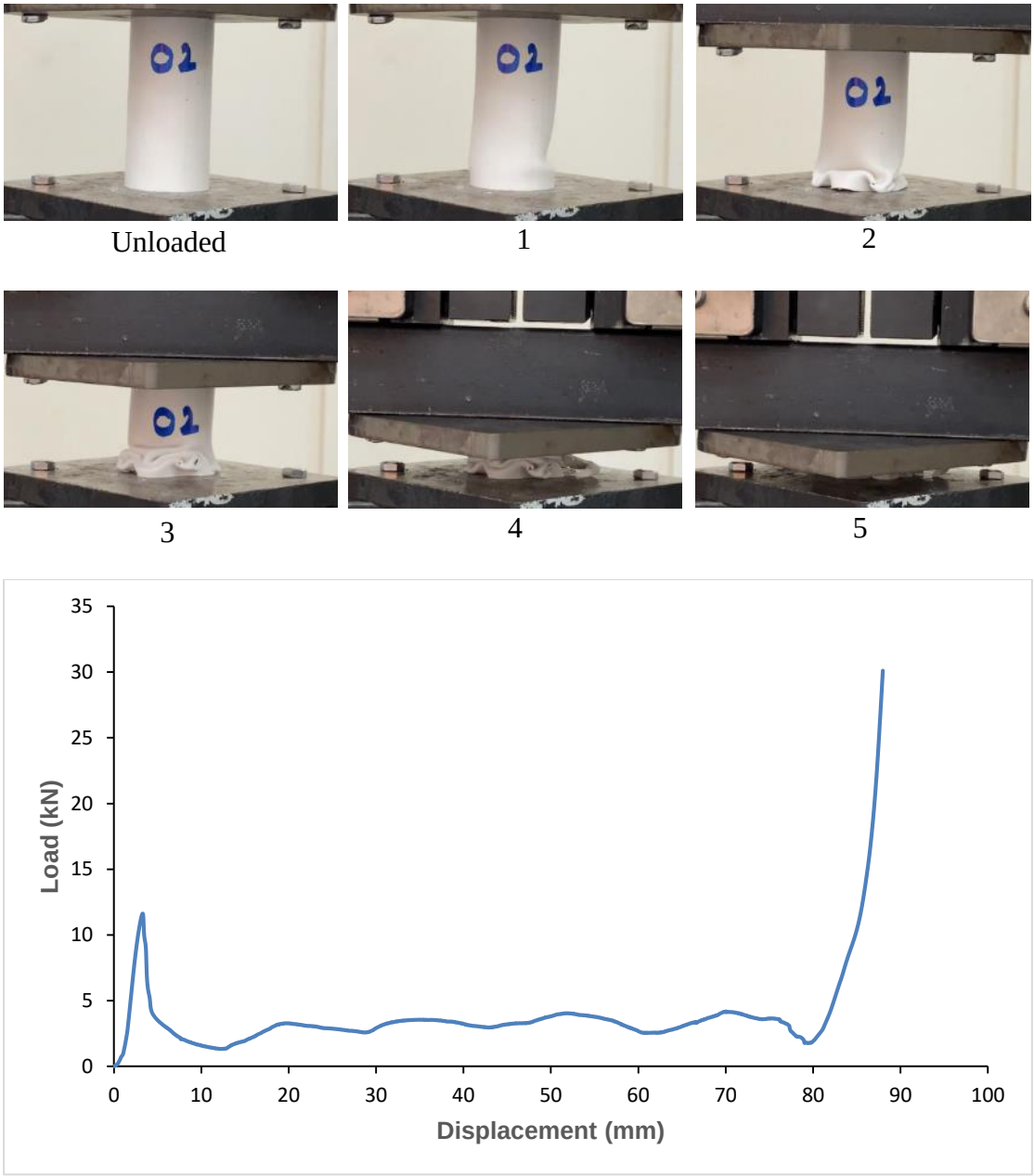

Figure 26. Images show the axial compression test of PVC pipe and the outcome load-displacement curve

The beginnings of the above figure show an increasing straight-line region, which is a direct proportion between the load and the displacement. This region is called the elastic region. In axial compression testing, the first peak that the specimen experiences its first turning drop point combined with the elastic region refers to the pre-crushing stage. Also, the initial peak force is the maximum load reached before the

turning drop point. The PVC specimen had a value of 11.63 kN approximately and occurred at a displacement of about 3.29 mm. Figure 26 and images 1-5 show the PVC tube's failure mechanism as progressive folding, which is an expected failure behavior for plastic tubes under compression and the characteristics of Mode-III failure. The stress generated from the compression on the PVC tube kept increasing enough to implement a local buckling on the tube wall, which formed a hinge, as shown in the image (1) from Figure 26. Also, it was noticed that the first hinge formation happened simultaneously when the initial peak force was reached. Then, a vast significant drop happened in the load-bearing capability, which indicated a catastrophic failure. After that, folds continued to form, which built up stresses in the walls, form hinges, and a subsequent decrease in load-bearing capability due to folding. However, the load kept rising and falling in stable margin for the second fold and onwards. Before the beginning of densification, the region referred to the post-crushing stage, which was displaced between 3.29 mm and 80 mm. This stage is represented in the images (2 to 50. The average load in this stage for the PVC tube was around 3.5 kN. After this stage, the densification stage will start, and the load will dramatically increase because the whole length of the tube is compressed, and the mass will continue to be compressed subsequently.

The first specimen in this thesis to be compared with the control sample is a non-grooved tube with GFRP wrapping from outside only with eight layers. As mentioned before, the total thickness of this sample after wrapping was 56 mm approximately. So, the GFRP layers have a thickness of around 3 mm with a wrapping angle of $\pm 45^{o}$. The load-displacement graph for this specimen after subjecting to quasi-static axial crushing test will be shown in Figure 27 below with corresponding images.

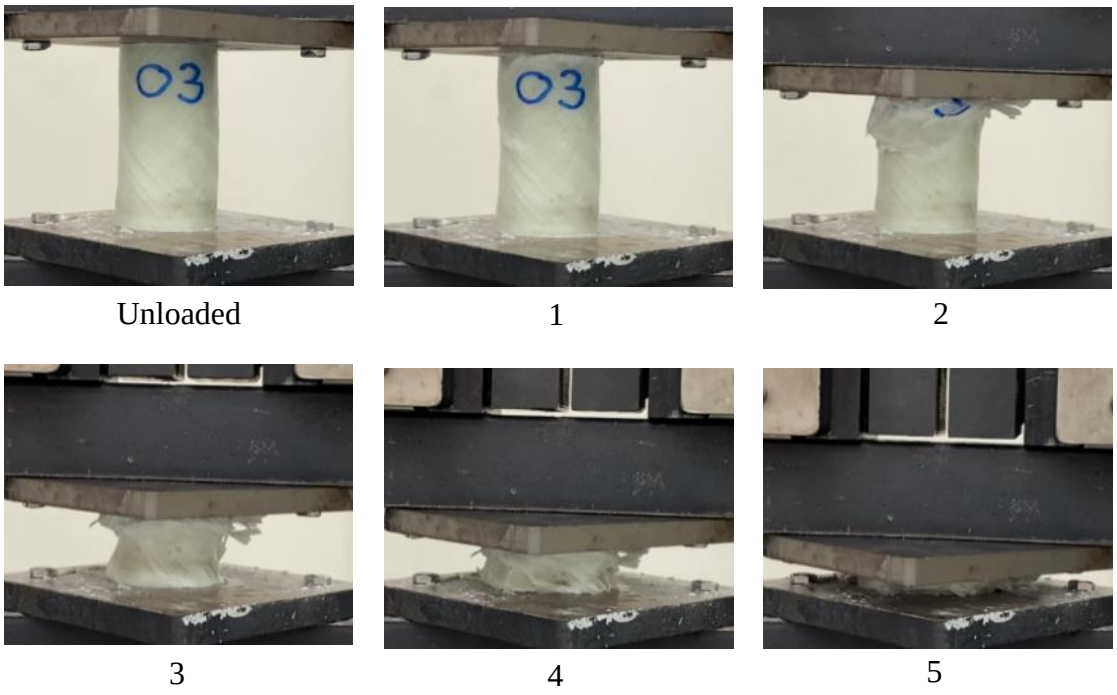

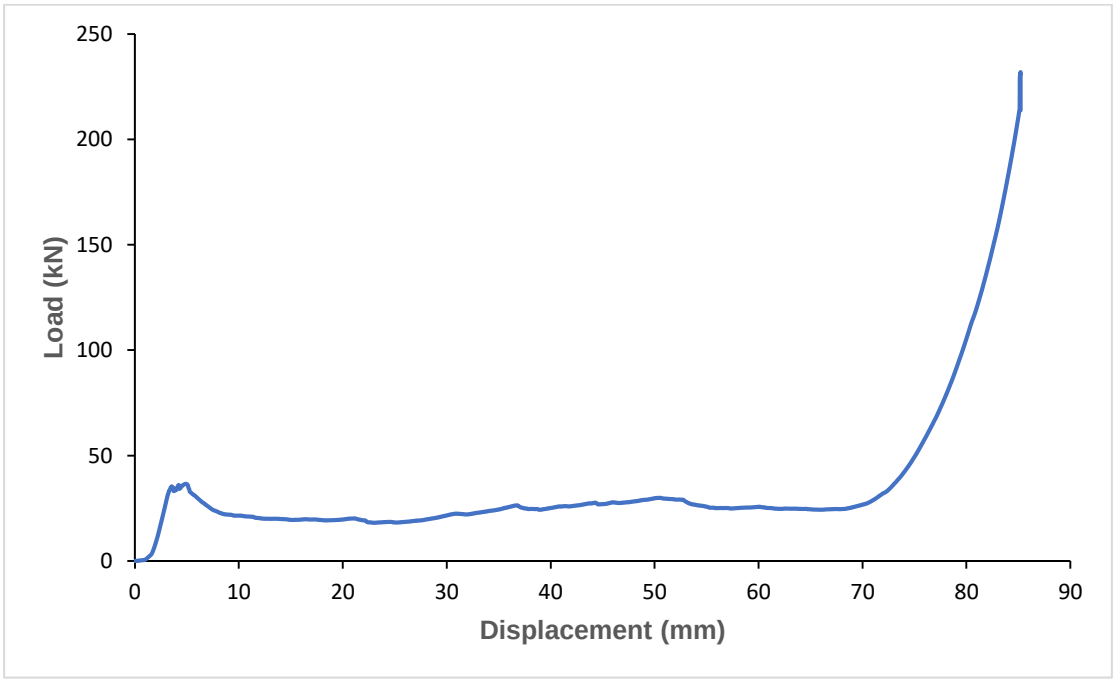

Figure 27. Images show the axial compression test of NGO specimen and the outcome load-displacement curve

Due to the global buckling, it was clear that the first mode of failure that occurred was Mode-III failure. The load fluctuated slightly at the initial peak force, forming a hinge with a maximum initial force of around 36.6 kN. This initial peak

happened at a displacement of 4.9 mm, approximately as an image (1) from the above figure showed. After the first fold, there was no dramatic drop in the load as the PVC sample. However, the load kept dropping until it reached the overall minimum amount of 18.1 kN at a displacement of 23 mm. The adhesion between the GFRP layers and the PVC inner tube collapsed, as shown in the image (2), explaining this drop in load-bearing capacity. This failure is identified as Mode-II failure in brittle composites. Then, the load raised slightly with a stable margin continuing Mode-III failure until the end of the post-crushing stage with mainly an average amount of 24.7 kN, which is represented in images (2-5). After that, the densification stage started till the end of the test. Overall, it can be observed that the performance of the NGO composite sample is way better than the PVC tube.

The second specimen in this thesis to be studied is a non-grooved tube with GFRP wrapping from outside with eight layers, and the wrapping angle is $\pm 45^{\circ}$. Also, this sample has a GFRP wrapping from inside, making the difference between this sample and the previous one. The inside wrapping was with four layers and had an angle of 90°. The total thickness and the outer GFRP thickness of this sample were equal to the previous sample. However, the inside wrapping will decrease the inner diameter, so this sample has an inner diameter equal to 43 mm, which concludes that the inner thickness of GFRP was around 1.5 mm. The load-displacement graph for this specimen after subjecting to quasi-static axial crushing test will be shown in Figure 28 below with corresponding images.

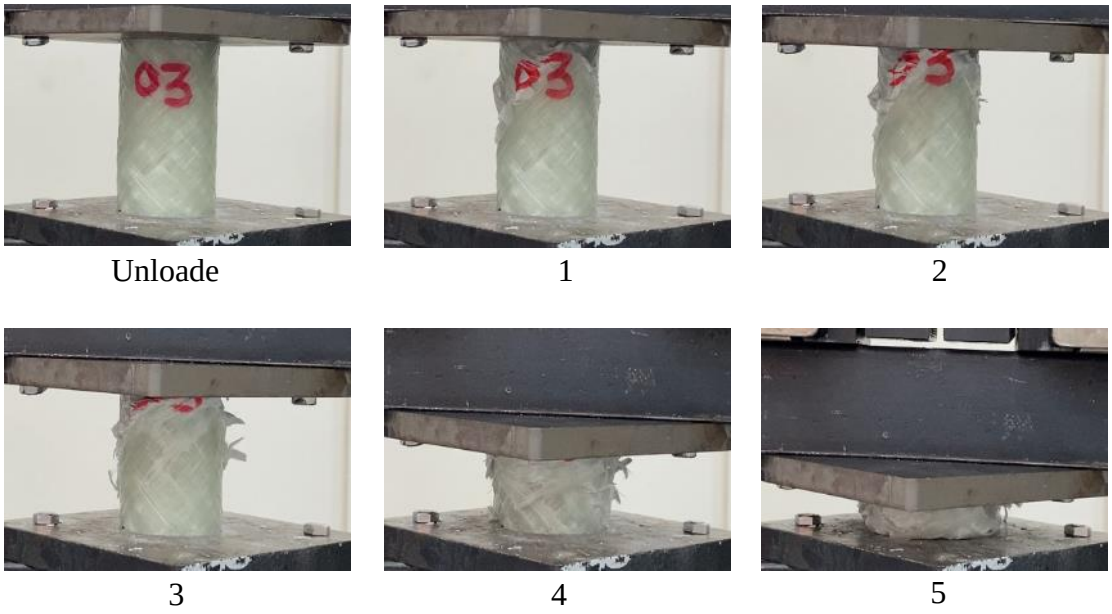

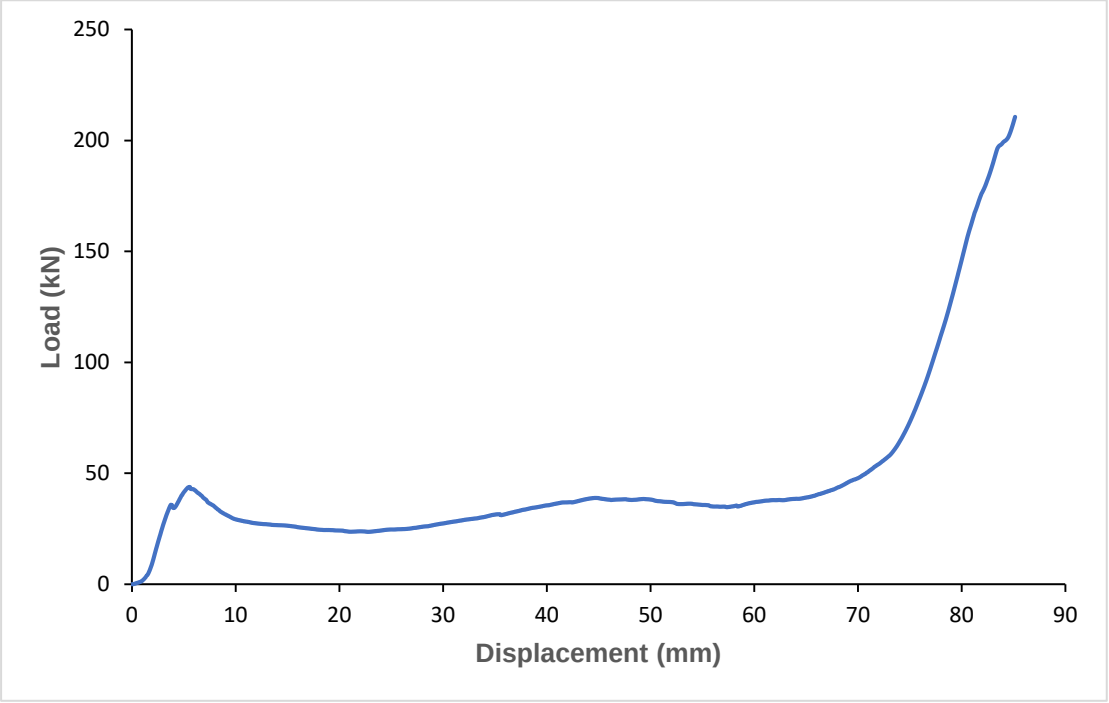

Figure 28. Images show the axial compression test of NGO specimen and the outcome load-displacement curve

In the beginning, due to transverse shear stress, a fracture plane was formed in the matrix material. This plane fully formed at a displacement of about 5.566 mm, with an initial peak load of 43.83 kN, as shown in image (2) from Figure 28. The cracks

formed were predominantly along the fiber orientation angle. Transverse shear was insufficient to initiate an entire separation across the fracture plane. However, it was enough to be the main reason for dropping the load-bearing behavior capacity and considerable cracking in the matrix material. Mode-II failure had these characteristics that caused such type of failure that affected bearing capacity until reaching a displacement of 26 mm approximately. After that, the axial crushing test surpassed the cracks. The specimen started to fold, which caused a significant increase in the load-bearing capacity reaching a local load peak with more stable crushing failure. It can be seen that the post-crushing stage split into two failure periods; Mode-II was the initial failure mode, then the rest were Mode-III. Lastly, the densification stage continued the compaction of the specimen.

This thesis's second category to be studied is grooved PVC tubes wrapped with GFRP. The circular grooves were made along the PVC tube in a specific pattern leaving a distance between each groove with 10 mm. The first specimen was wrapped from outside only, and the other specimen was wrapped from inside and outside. Starting with the specimen that wrapped from outside only, the outer diameter of the PVC itself variate between 49 or 50 mm due to 1 mm grooves made before. Also, the outer diameter of the wrapping was 55 mm. Hence, the thickness of 8 layers of fiberglass is 3 mm almost, and the wrapping angle was ±45º as usual; the load-displacement graph for this grooved specimen after subjecting to quasi-static axial crushing test will be shown in Figure 29 below with corresponding images.

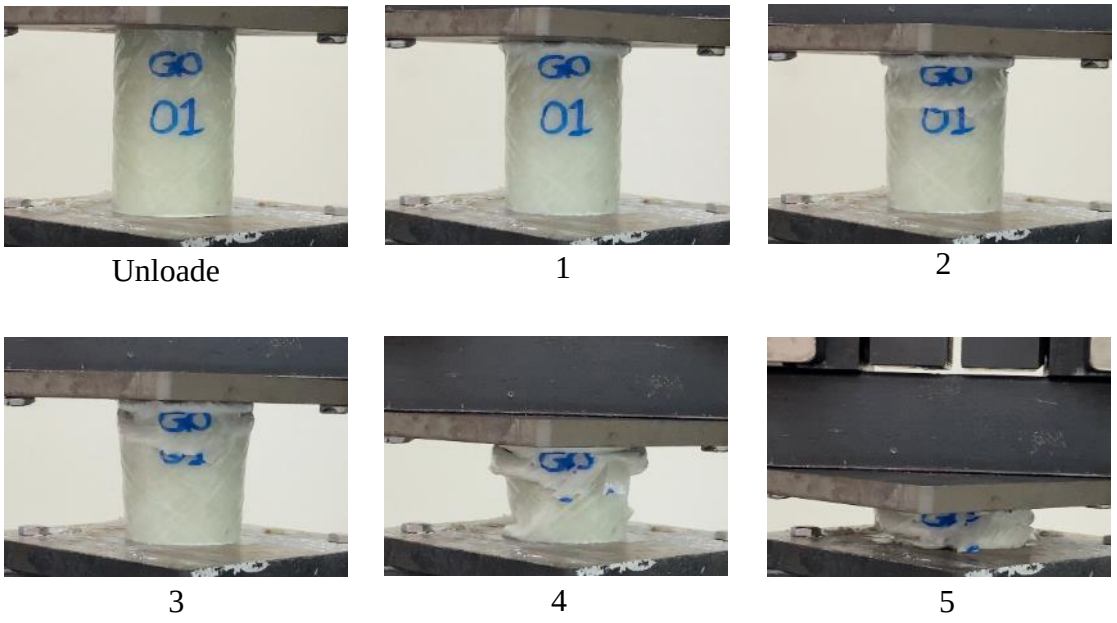

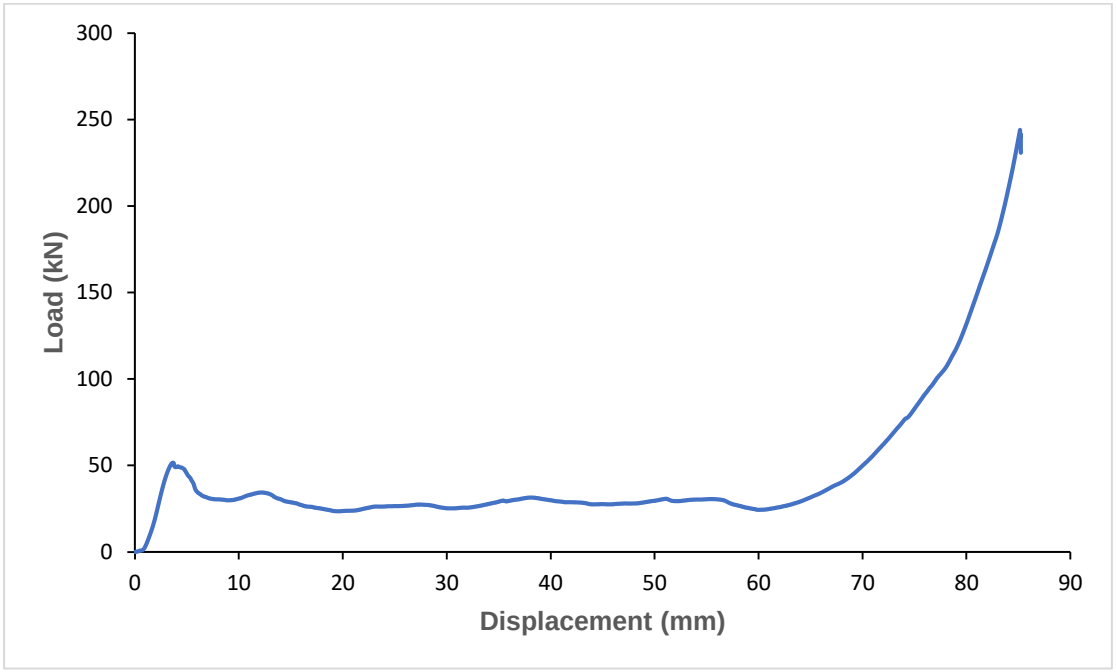

Figure 29. Images show the axial compression test of the GO specimen and the outcome load-displacement curve

First, the specimen started folding smoothly, representing the mode-I failure behavior with a mushroom appearance. The image (1) from Figure 29 coincided with an initial peak load of 51.6 kN, which happened early at a displacement around 3.7 mm. Then it was observed that the drop occurred in two stages, one after the other. The first drop is the beginning of the post-crushing stage. The second drop happened due to most

of the specimen's horizontal fracture in the midle, as shown in image (2). The crack formed were not along the fiber orientation angle. However, the transverse shear stress was enough to separate the reinforcement along the fracture surface. This failure was sufficient to be the main reason for the reduced load capacity. Significant cracking of the matrix material reached a minimum load absorbed of 23.5 approximately occurred at displacement around 20 mm. After that, the load started rising stably until the end of the post-crushing stage. Lastly, the densification stage continued the compaction of the specimen.

The second specimen in this category is a grooved PVC pipe wrapped inside and outside with GFRP. The outer wrapping with eight layers with an angle of ± 45º as mentioned before. The inner wrapping had four layers in 90˚. The outer diameter was equal to the previous specimen and had the same thickness, which is 3 mm almost. Knowing the inner diameter and the original diameter of the PVC itself, the thickness of the inner GFRP wrapping is around 1.5 mm. The load-displacement behavior for this specimen is shown in Figure 30.

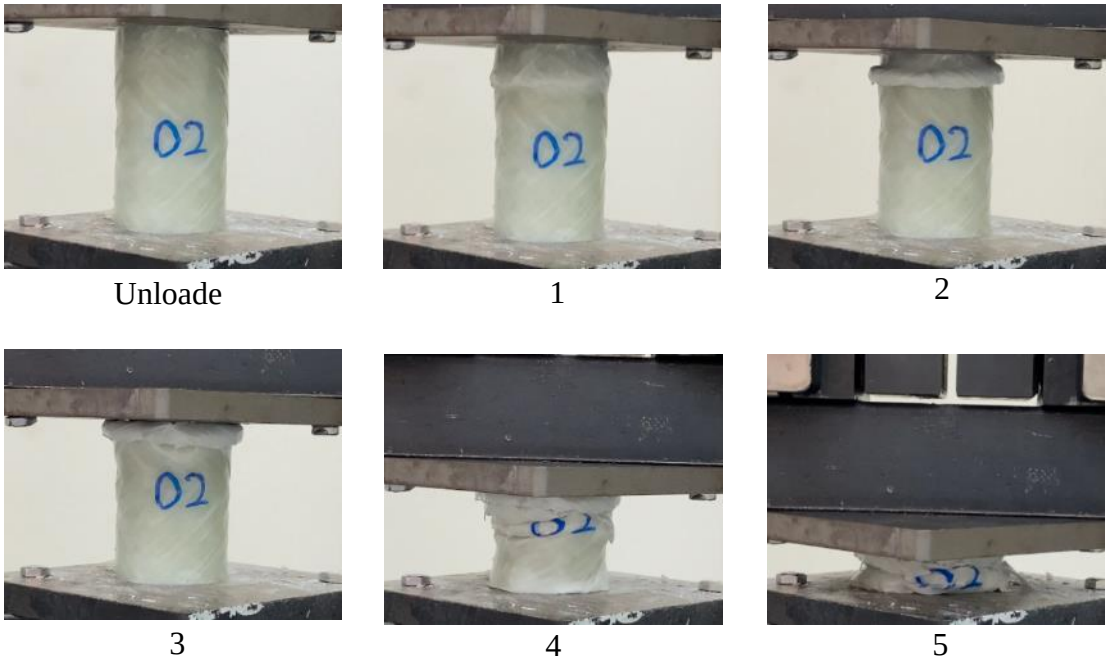

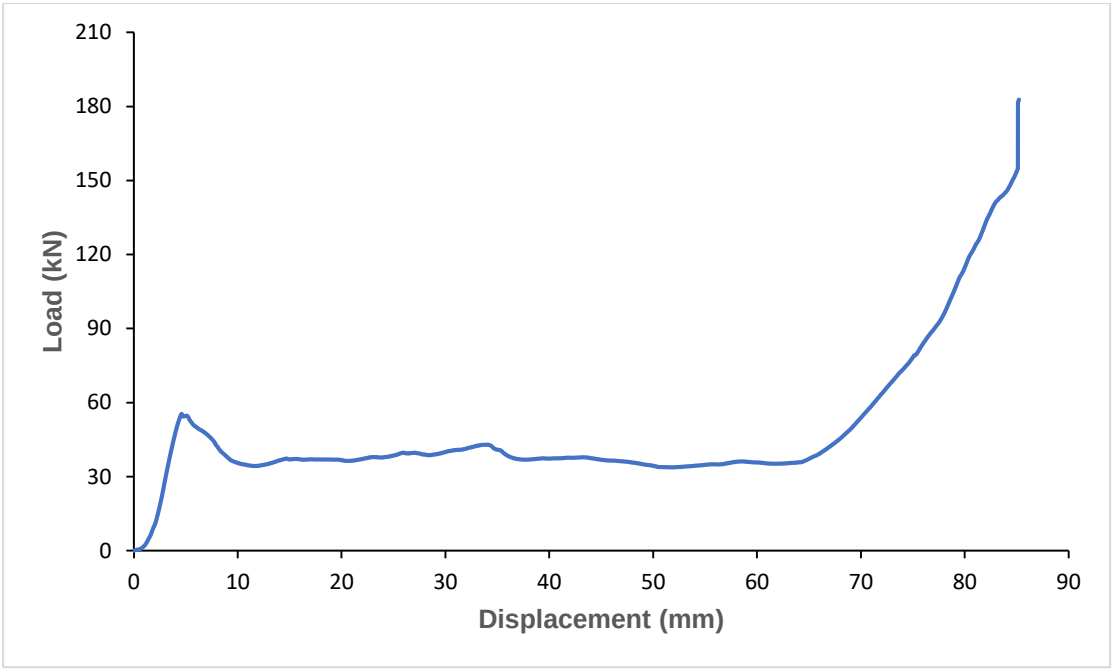

Figure 30. Images show the axial compression test of the GIO specimen and the outcome load-displacement curve

In the beginning, a circumferential crack occurred at the top third of the composite tube because of the build-up of transverse shear stress, as shown in the image (1) from Figure 30. This crack developed at an initial peak load of 53.7 kN and a displacement of 5.278 mm approximately. Also, the specimen was split into two

sections. The top section started to compact alone without penetrating the bigger bottom section. As a result, the load-bearing capacity did not significantly drop as an expected failure. Instead, it moderately dropped, reaching an average of 37.2 kN, and the compaction process continued until it reached the circumferential crack. Then, the big bottom section started to deform, which led to a slight increase in load-bearing capacity in a displacement range between 28 to 35 mm. During the post-crashing stage, the overall behavior of load-bearing capacity was stable. Lastly, the densification stage continued the compaction of the specimen.

Several comparisons were made between the specimens to study the behavior of different aspects mentioned before on the load-bearing capacity. The first comparison examines the effect of wrapping GFRP from outside only or inside and outside. The second comparison studies the behavior of grooved specimens. The third comparison studies the effect of grooving. The fourth comparison shows the behaviors of the specimens that wrapped from inside and outside. Finally, a comparison in which an overall analysis has been conducted identifies the best design. Figure 31 shows the load-displacement curves of the NGIO and NGO samples under the compression test.

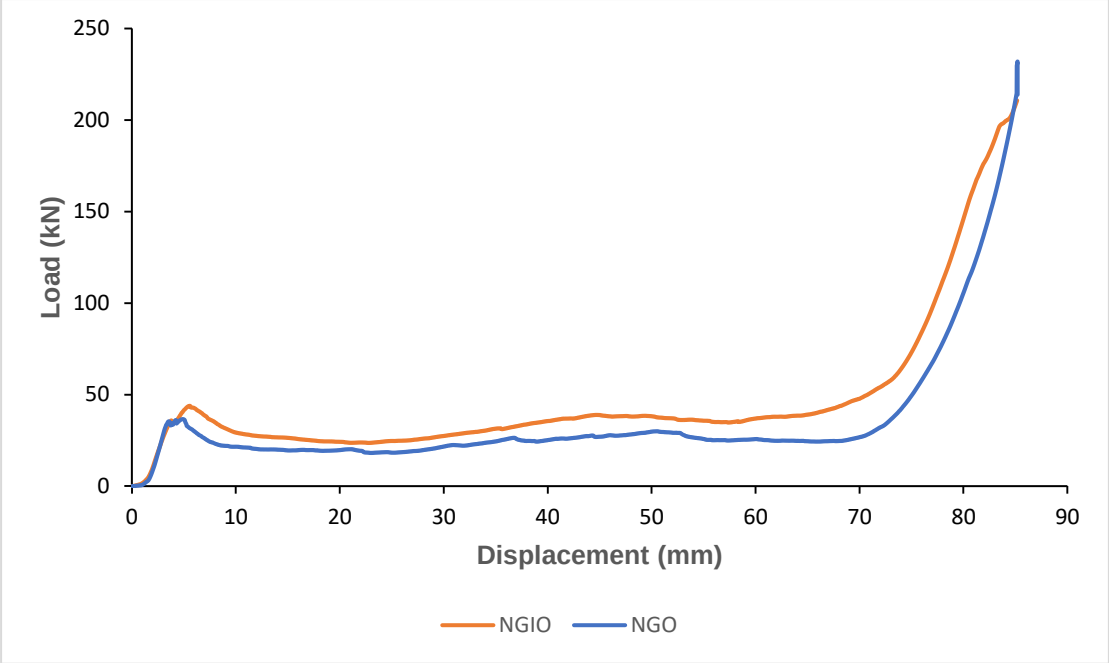

Figure 31. The load-displacement curve of the non-grooved samples under axial compression test

It was observed that the two non-grooved specimens started exactly with the same behavior, but the NGIO specimen reached a higher initial peak around 43.83 kN when the NGO specimen reached 36.6 kN. Also, the initial peak of NGIO occurred at a further distance from the NGO. During the post-crushing stage, both specimens were analogous on periods of dropping and raising, but the NGIO showed a lower dropping rate after the initial load peak. Overall, outer and inner wrapping with GFRP raised the load-bearing capacity by a mild percentage without disturbing the behavior of the composite tube while exposed to crushing load.

Figure 32 shows the load-displacement curves of both grooved specimens, the GIO and the GO samples, under the compression test.

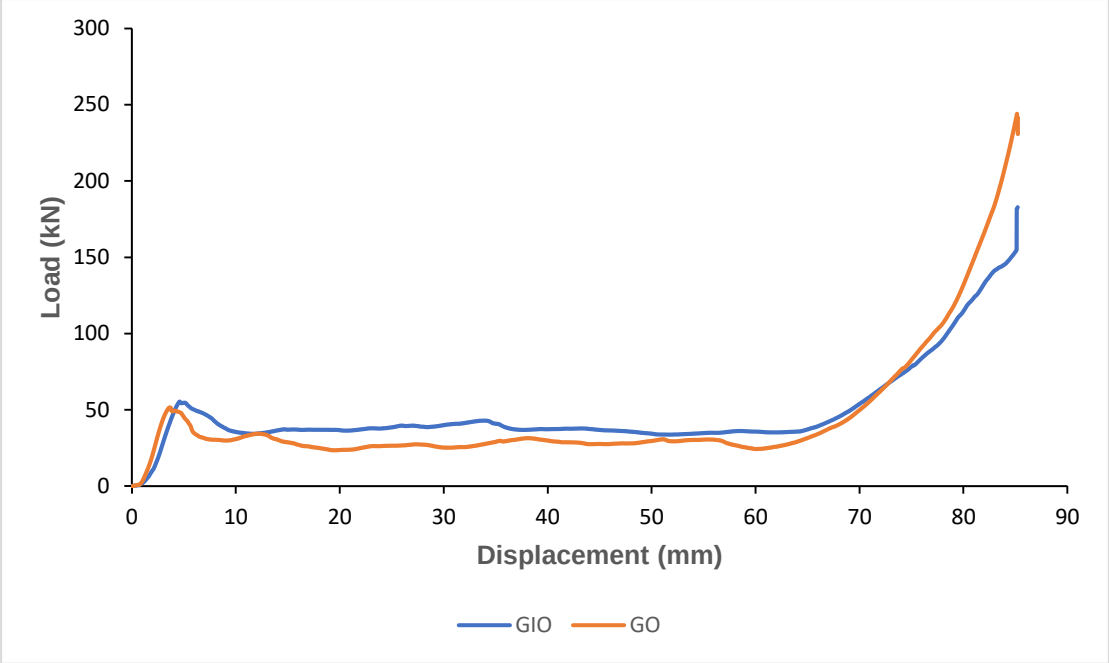

Figure 32. The load-displacement curve of the grooved samples under axial compression test

For these two specimens, the GIO reached an initial load peak slightly more than the GO and occurred at a further distance. GIO had 55.4 kN, and GO had 51.6 kN. Both showed an intimate performance in the post-crushing stage but with an advantage for the GIO between 13 to 35 mm. This finding supports the previous outcomes of wrapping internally and externally to have a moderate percentage of improvement in load-bearing capacity.

Specimens wrapped similarly will be compared together to examine the effect of grooving on the load-bearing capacity. Figure 33 shows the load-displacement curves of both specimens wrapped externally: the NGO and the GO samples after exposure to the compression test.

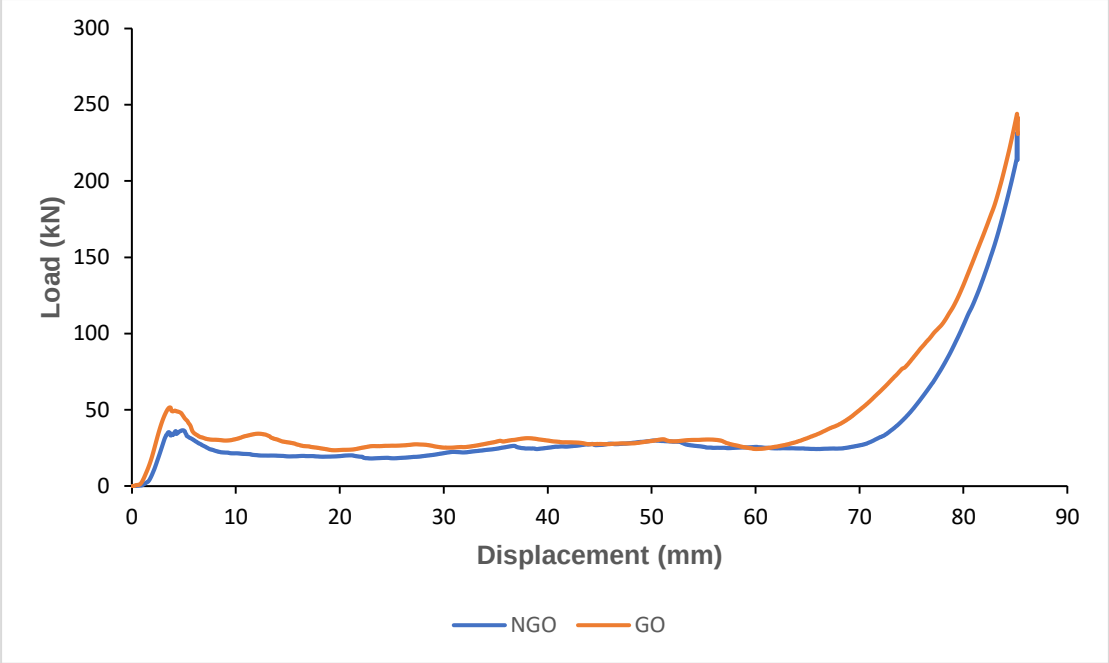

Figure 33. The load-displacement curve of the externally wrapped samples under axial compression test

From the initial observation for the above figure, it can be observed that the grooved sample reached a noticeably higher initial peak load compared to the non-grooved. The grooved specimen had an initial peak load of 51.6 kN, but the non-grooved had only 36.6 kN. However, both specimens had similar behavior and values in the post-crushing stage, with a minor advantage for the grooved specimen.

The load-displacement curves for the compression test of both NIGO and GIO specimens, which wrapped externally and internally, will be shown in Figure 34.

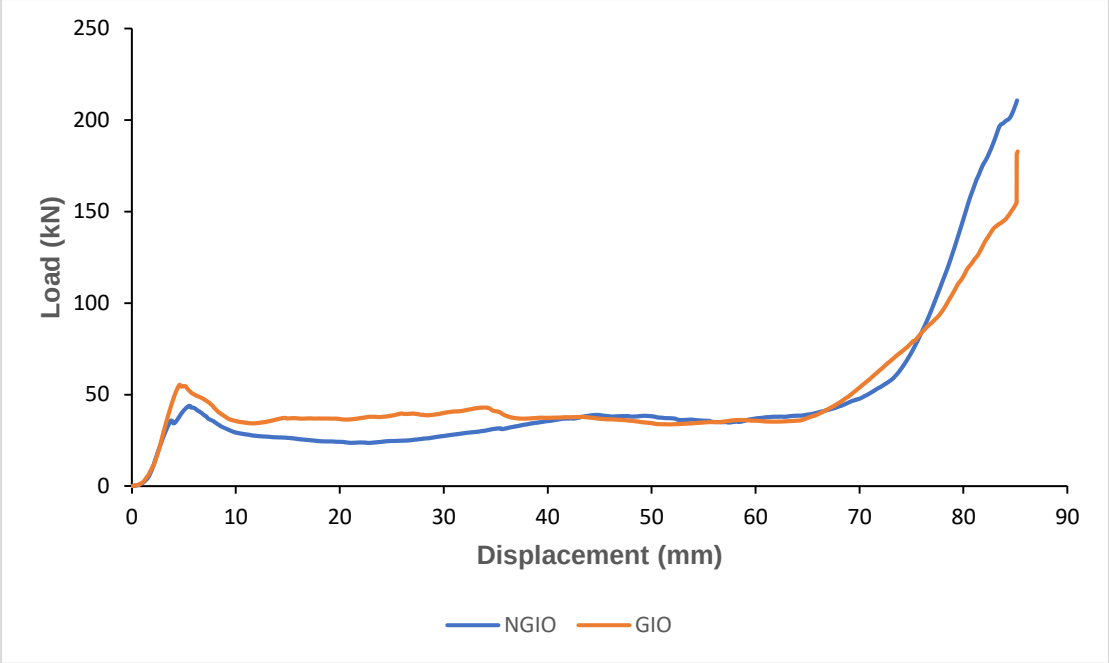

Figure 34. The load-displacement curve of the externally & internally wrapped samples under axial compression test

As the previous comparison, the grooved sample had an initial peak load much higher than the non-grooved. The grooved sample had an advantage in the first half for the post-crushing stage, but both were almost equal in the second half. So, the primary modification of the grooving can be concluded in improving the pre-crushing stage for the specimens, which shows that grooving is a minor way to improve the load-bearing behavior slightly.

All of the composite tubes' load-displacement curves with different wrapping locations and grooving were plotted alongside the PVC graph as the load-displacement curve shown in Figure 35.

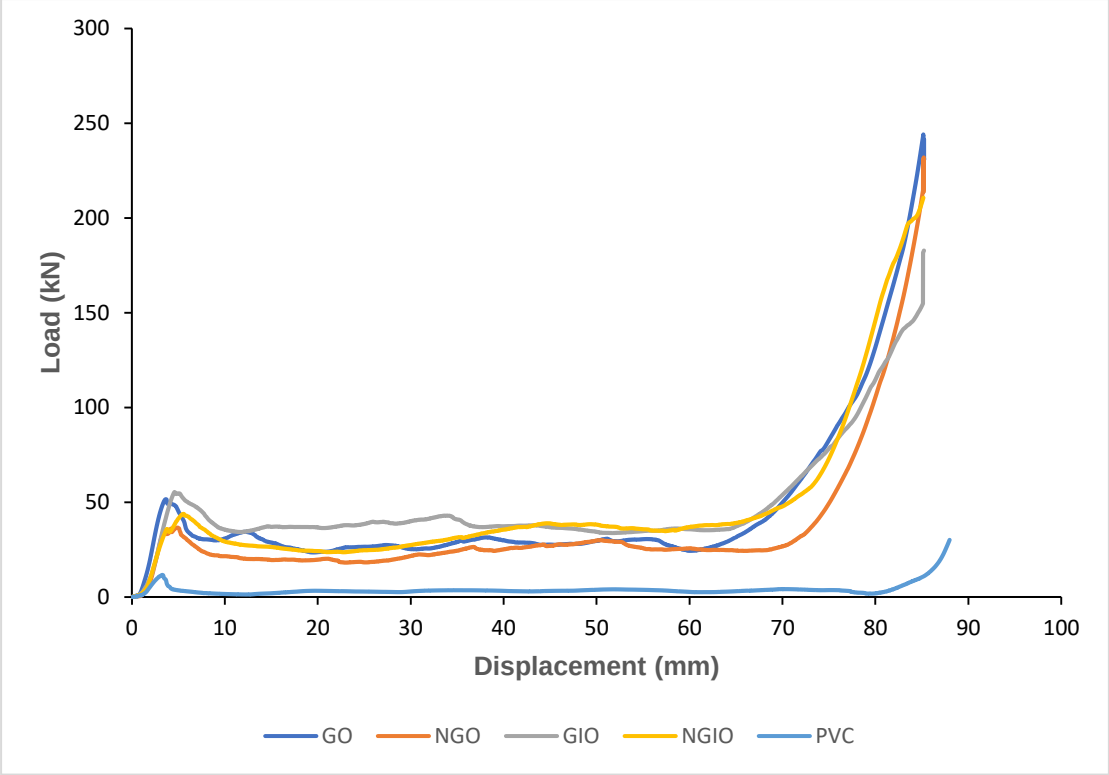

Figure 35. The load-displacement curve of all GFRP reinforced samples and the PVC sample under axial compression test

The load-bearing capacity for all GFRP overwrapped specimens is much higher than the PVC, as shown in Figure 35. PVC tubes cannot be compared with any GFRP tubes because they are many times higher. The initial peak load for the PVC was around 11.63 kN, while the NGO, the nearest one to the PVC, had an initial peak load of 36.6 kN. During the pre-crushing stage, the GIO sample had the highest value with a moderate initial turning point, while the NGO was the lowest. In general, as the samples are wrapped internally and externally, the higher load-bearing capacity to acquire. Both non-grooved samples reached the lower peak at the beginning of the post-crushing stage and then increased. Finally, to observe more detailed variations, crush force efficiency and energy absorption capabilities will be discussed and explained below.

4.2. Influence on Crush Force Efficiency

As shown in Table 5, the crush force efficiency for all the grooved and non-grooved samples was dramatically higher than the crush force efficiency for the PVC tube. The grooved externally overwrapped tube had the least crush force efficiency and was still higher than the CFE for the PVC by 2.5 times approximately. The highest CFE found was the non-grooved externally and internally overwrapped tube with a value of 0.7873. Also, it was noticed that the CFE of non-grooved specimens is barely higher than its rival sample from the grooved specimens. Moreover, it was noticed that the instantaneous crush force efficiency within 0.1 of the ideal for the non-grooved and grooved specimens was higher than the PVC. Nearly all the samples had the same iCFE except the grooved externally and internally overwrapped specimen that had a percentage of 58.26 %. Therefore, it cannot be concluded that the grooving will disturb the samples' stability or negatively affect the CFE.

Table 5. Samples Result of CFE and %iCFE within 0.1 from Ideal

Samples	CFE	% iCFE ±0.1 from Ideal
PVC	0.2541	34.11
NGO	0.6403	45.94
NGIO	0.7873	46.97
GO	0.6092	43.59
GIO	0.7433	58.26

4.3. Influence on Energy Absorption Capability

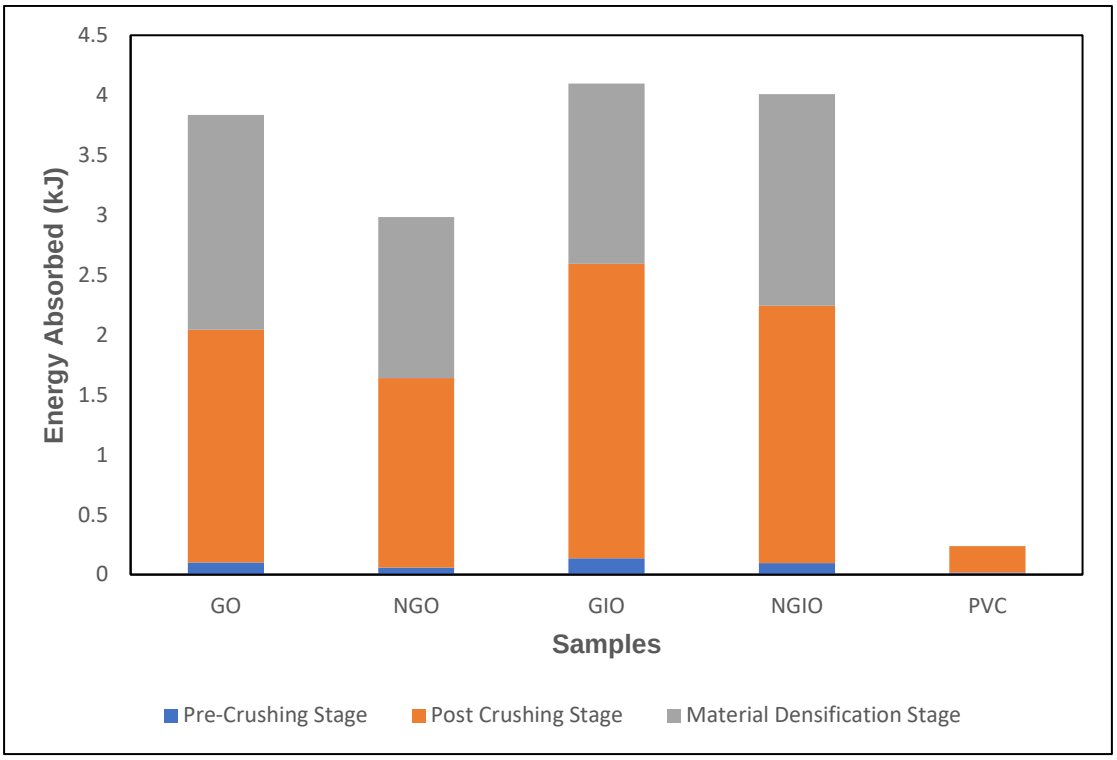

Figure 36. Energy absorbed by the wrapped grooved, wrapped non-grooved, and PVC tubes

Figure 36 shows the energy absorbed by the grooved, non-grooved samples and the PVC. The load-bearing curves were utilized to evaluate the area under their curves. The amount of energy absorbed will be determined by calculating the area under the load-displacement curves. The amount of energy absorbed was represented in different colors for ease of comparison. It can be seen that the PVC tube had inconsiderable energy absorbed in the densification stage. It is barely absorbed energy in the pre-crushing stage and much less energy absorbed in the post-crushing stage than any other GFRP overwrapped specimen. Comparing the energy absorbed at pre-crushing and post-crushing stages between the reinforced specimens, the non-grooved sample that wrapped externally only was the lowest. During the pre-crushing stage, the NGO

reinforced sample absorbed more than triple energy than the PVC, almost 0.059 kJ for the NGO and 0.016 kJ for the PVC. During the post-crushing stage, the NGO reinforced sample absorbed more than seven times more energy than the PVC, almost 1.58 kJ for the NGO and 0.22 kJ for the PVC. It was noticed that the specimens wrapped externally and internally absorbed energy in both stages higher than the rival sample that only wrapped externally. For example, the NGIO absorbed about 0.096 kJ of energy in the pre-crushing stage, which is 63.5% higher than the NGO, and 2.15 kJ of energy in the post-crushing stage which is 36% higher than the NGO.

Moreover, it was noticed that the grooved sample absorbed more energy than its rival from the non-grooved samples, especially in the pre-crushing stage. Therefore, the blue color in the graph showed higher values for the grooved compared to the non-grooved. For example, the GO sample absorbed about 0.102 kJ of energy in the pre-crushing stage, almost 75% higher than the NGO. However, it is essential to consider the weight of each different sample to represent the specific energy absorbed for each reinforced sample and the PVC, so before carrying out compression tests, the masses of all samples were measured. Figure 37 below shows the specific energy absorbed for all tested samples.

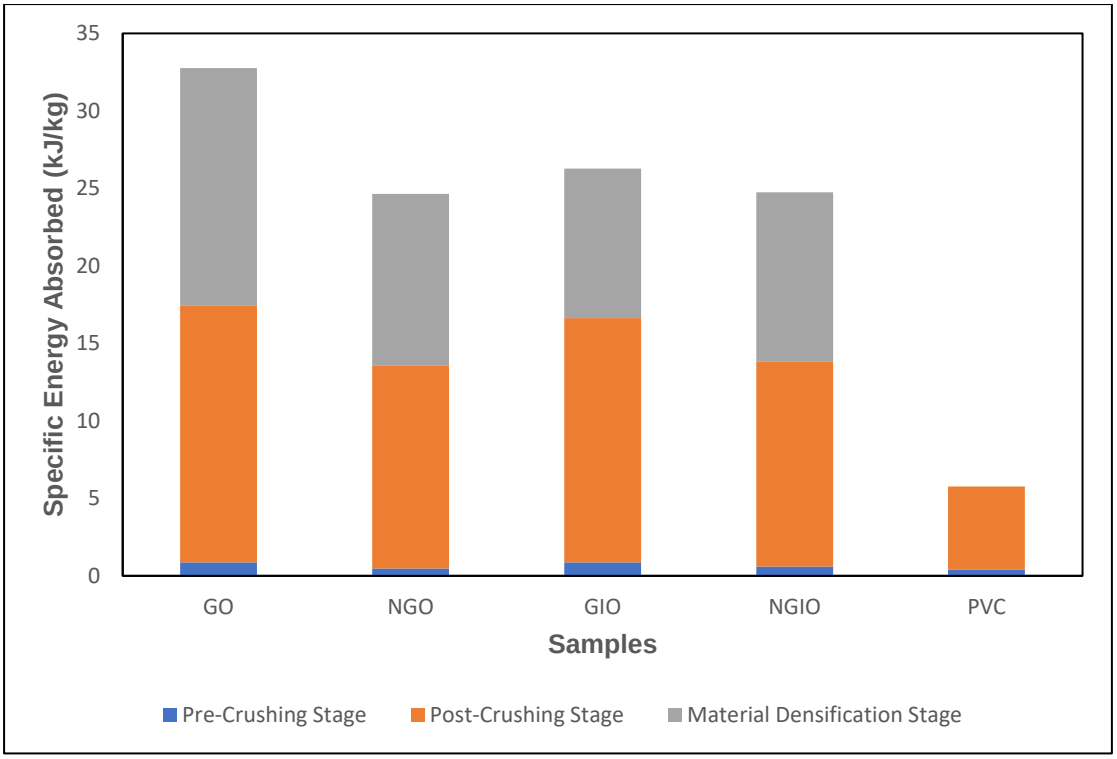

Figure 37. The specific energy absorbed by the wrapped grooved, wrapped non-grooved, and PVC tubes

Figure 37 shows the specific energy absorbed by the grooved, non-grooved samples and the PVC, considering the masses that can affect the three stages of absorbing. Even though the PVC has a very light mass, it still has much less specific energy absorbed in the post-crushing stage than any other tested samples. However, the PVC pre-crushing specific energy can only be compared to the non-grooved samples. Also, the non-grooved wrapped externally only was the lowest between the reinforced samples with specific absorbed energies at pre-crushing and post-crushing stages. During the pre-crushing stage, the NGO reinforced sample absorbed specific energy 23.5 % more than the PVC, almost 0.486 kJ/kg for the NGO and 0.393 kJ/kg for the PVC. During the post-crushing stage, the NGO reinforced sample absorbed specific energy more than double that of the PVC, almost 13.07 kJ/kg for the NGO and 5.372 kJ/kg for the PVC. After considering the masses, the importance of samples that wrapped externally and internally almost disappeared.

On the contrary, there is an advantage now for the GO sample that preceded all other samples even though it wrapped externally only. Moreover, the advantage of the grooved samples over its rival from the non-grooved samples in absorbing more specific energy in the pre-crushing stage is still there. For example, the GO sample absorbed about 0.870 kJ/kg of specific energy in the pre-crushing stage, almost 80% higher than the NGO.

4.4. Selection of Best Performance Tested Tube

The tested tube with the best performance will be selected in this section. Crashworthiness characteristics are the weighting terms for the scoring system. Table 6 will show the scoring parameters with their value, the ranking of each tested tube for every parameter, and the final score for each tested tube. The crush force efficiency was given the most weight, as seen from the weighting. The specific energy absorbed came next, followed by the load-bearing capacity. The cost was also addressed, and it was shown to be directly proportional to the mass and presence of grooving of the composite tubes.

According to Table 6, the GIO tube was rated as the top performing composite tube, and NGIO came as the second. These findings conclude the importance of wrapping externally and internally with the glass fiber filament. The GO sample was the best specimen studied in absorbing energy, but its CFE and iCFE were unsatisfactory and affected its total score. On the other hand, the GIO sample came second in absorbing energy, but because of its superiority in CFE and iCFE, the GIO sample preceded the other samples.

Table 6. Best performance selection of tested tubes

Samples	Cost [/1]		Load at 1st Failure [/1]		Pre-crushing Energy [/2]		Post-crushing Energy [/4]		Densification Energy [/1]		CFE [/6]		% iCFE ±0.1 from Ideal [/10]		Total Score [/25]
	Rank	Mass/Grooving (kg)	Rank	(kN)	Rank	SE (kJ/kg)	Rank	SE (kJ/kg)	Rank	SE (kJ/kg)	Rank	(Unitless)	Rank	%	
PVC	1	0.041/No	5	11.63	5	0.3934	5	5.3721	5	0	5	0.2541	5	34.11	01.00
NGO	2	0.121/No	4	36.6	4	0.4860	4	13.072	2	11.088	3	0.6403	3	45.94	11.25
NGIO	4	0.162/No	3	43.83	3	0.5933	3	13.253	3	10.892	1	0.7873	2	46.97	17.75
GO	3	0.117/Yes	2	51.6	1	0.8701	1	16.594	1	15.306	4	0.6092	4	43.59	12.25
GIO	5	0.156/Yes	1	53.7	2	0.8693	2	15.595	4	9.6360	2	0.7433	1	58.26	20.25

Total Score Equation: (To be applied for each parameter and sum up the values for each tested tube)

$$Score\ for\ parameter = Points\ assigned\ to\ parameter - [Points\ assigned\ to\ parameter \times \left(\frac{rank - 1}{5 - 1}\right)]$$

CHAPTER 5: CONCLUSION AND RECOMMENDATIONS

This thesis implemented four different GFRP composite tubes from the PVC tube. Non-grooved PVC tube wrapped with glass fiber externally, non-grooved PVC tube wrapped externally and internally, grooved PVC tube wrapped externally, and grooved tube that wrapped externally and internally. The external wrapping angle was ±45º with eight layers of glass fiber, and the internal wrapping angle was 90ºwith four layers of glass fiber. The matrix material was epoxy resin with a 30 to 100 ratio of hardener to epoxy. After that, the composite tubes and the PVC tube were exposed to axial quasi-static compression tests to verify the effect of grooving and wrapping on the crashworthiness behavior. Finally, various comparisons were made between the composite tubes and the PVC tube to select the best performing tube.

5.1. Conclusion

The following conclusions were reached based on the experimental results:

i. The load-bearing capacity, crush force efficiency, instantaneous crush force efficiency, energy absorption, and specific energy absorption capabilities for the composite GFRP tubes are much higher than the PVC tube alone during the compression test.

ii. Transverse shear, matrix cracking, and buckling were the frequent failure mechanisms exhibited by the GFRP composite tubes and the PVC tube.

iii. Regardless of the wrapping, the grooved samples had an initial peak load more significant than the non-grooved samples, which led to higher energy absorption and specific energy absorption in the pre-crushing stage.

iv. Regardless of the grooving, the samples wrapped externally and internally had

higher crush force efficiency and instantaneous crush force efficiency than those wrapped externally only.

v. In selecting the best performance test tube, the grooved composite tube wrapped externally and internally got the highest overall ranking point, 20.25 out of 25.

5.2. Recommendations for Future Work

Non-linear finite element analysis is recommended for determining the best performing composite tube in terms of crashworthiness characteristics among the composite tubes examined in this study. Despite the importance of the experimental work, finite element analysis is very important. Below are factors that were not considered in this study but may be investigated in future studies:

i. Inner tubes with different materials, such as aluminum which has been explored widely, could be used.

ii. Foam cores inside the tubes could be compared with the samples wrapped internally with glass fiber.

iii. For each sample, the number of GFRP layers may be varied, and layers with different fiber orientations can be investigated.

iv. Other reinforcing materials or matrix materials can be explored as well.

REFERENCE

[1] S. Duan, Y. Tao, X. Han, X. Yang, S. Hou, and Z. Hu, “Investigation on structure optimization of crashworthiness of fiber reinforced polymers materials,” *Compos. Part B Eng.*, vol. 60, pp. 471–478, Apr. 2014, doi: 10.1016/j.compositesb.2013.12.062.

[2] “Global status report on road safety 2018,” *World Health Organization*. Available: https://www.who.int/violence_injury_prevention/road_safety_status [Accessed: 29-May-2022].

[3] J. D. D. Melo, A. L. S. Silva, and J. E. N. Villena, “The effect of processing conditions on the energy absorption capability of composite tubes,” *Compos. Struct.*, vol. 82, no. 4, pp. 622–628, Feb. 2008, doi: 10.1016/j.compstruct.2007.03.001.

[4] G. C. Jacob, J. F. Fellers, S. Simunovic, and J. M. Starbuck, “Energy absorption in polymer composites for automotive crashworthiness,” *J. Compos. Mater.*, vol. 36, no. 7, pp. 813–850, 2002, doi: 10.1177/0021998302036007164.

[5] A. Kaw, *Mechanics of Composite Materials*, Second edi. CRC PRESS Taylor & Francis Group, 2006.

[6] S. Khadem Moshir, S. Van Hoa, and F. Shadmehri, “Stress analysis of elliptical composite tubular beams using a meshless dimensional reduction method,” *Compos. Struct.*, vol. 274, Oct. 2021, doi: 10.1016/j.compstruct.2021.114323.

[7] A. G. Mamalis, D. E. Manolakos, G. A. Demosthenous, and M. B. Ioannidis, “Analysis of Failure Mechanisms Observed in Axial Collapse of Thin-Wailed Circular Fibreglass Composite Tubes,” 1996.

[8] D. Hu, C. Zhang, X. Ma, and B. Song, “Effect of fiber orientation on energy absorption characteristics of glass cloth/epoxy composite tubes under axial

quasi-static and impact crushing condition," *Compos. Part A Appl. Sci. Manuf.*, vol. 90, pp. 489–501, Nov. 2016, doi: 10.1016/j.compositesa.2016.08.017.

[9] A. A. S. Abosbaia, E. Mahdi, A. M. S. Hamouda, and B. B. Sahari, "Quasi-static axial crushing of segmented and non-segmented composite tubes," *Compos. Struct.*, vol. 60, no. 3, pp. 327–343, 2003, doi: 10.1016/S0263-8223(02)00341-0.

[10] A. S. Abosbaia, E. Mahdi, A. M. S. Hamouda, B. B. Sahari, and A. S. Mokhtar, "Energy absorption capability of laterally loaded segmented composite tubes," *Compos. Struct.*, vol. 70, no. 3, pp. 356–373, Sep. 2005, doi: 10.1016/j.compstruct.2004.08.039.

[11] E. Mahdi, A. M. S. Hamouda, B. B. Sahari, and Y. A. Khalid, "2003Effect of hybridisation on crushing behaviour of carbon-glass fibre-epoxy circular-cylindrical shells.pdf," vol. 132, pp. 49–57, 2003.

[12] A. G. Facca, M. T. Kortschot, and N. Yan, "Predicting the elastic modulus of natural fibre reinforced thermoplastics," *Compos. Part A Appl. Sci. Manuf.*, vol. 37, no. 10, pp. 1660–1671, Oct. 2006, doi: 10.1016/j.compositesa.2005.10.006.

[13] K. Okubo, T. Fujii, and Y. Yamamoto, "Development of bamboo-based polymer composites and their mechanical properties," in *Composites Part A: Applied Science and Manufacturing*, Apr. 2004, vol. 35, no. 3, pp. 377–383. doi: 10.1016/j.compositesa.2003.09.017.

[14] C. W. Isaac and C. Ezekwem, "A review of the crashworthiness performance of energy absorbing composite structure within the context of materials, manufacturing and maintenance for sustainability," *Composite Structures*, vol. 257. Elsevier Ltd, Feb. 01, 2021. doi: 10.1016/j.compstruct.2020.113081.

[15] F. C. Campbell, "Introduction to Composite Materials and Processes: Unique

Materials that Require Unique Processes," in *Manufacturing Processes for Advanced Composites*, 2004, pp. 1–37. doi: 10.1016/b978-185617415-2/50002-2.

[16] M. Knight and D. Curliss, "Marine Composites-page 115." p. 377, 1999.

[17] M. Kassa, T. Daniel, and A. Ato, "Fabrication and Mechanical Property Characterization of Sisal fiber Reinforced Epoxy Resin Composite Material for Automotive body Application," 2015. doi: 10.13140/RG.2.2.16765.82407.

[18] J. Njuguna, K. Pielichowski, and J. Fan, *Polymer nanocomposites for aerospace applications*. Woodhead Publishing Limited, 2012. doi: 10.1533/9780857096241.3.472.

[19] J. S. Jayan, S. Appukuttan, R. Wilson, K. Joseph, G. George, and K. Oksman, "1 - An introduction to fiber reinforced composite materials," in *Woodhead Publishing Series in Composites Science and Engineering*, K. Joseph, K. Oksman, G. George, R. Wilson, and S. B. T.-F. R. C. Appukuttan, Eds. Woodhead Publishing, 2021, pp. 1–24. doi: https://doi.org/10.1016/B978-0-12-821090-1.00025-9.

[20] F. C. Campbell, "Structural Composite Materials," *Struct. Compos. Mater.*, 2010, doi: 10.31399/asm.tb.scm.9781627083140.

[21] K. K. Chawla, "Glass Fibers," M. B. T.-E. of M. T. C. and G. Pomeroy, Ed. Oxford: Elsevier, 2016, pp. 676–680. doi: https://doi.org/10.1016/B978-0-12-818542-1.02325-0.

[22] M. Derradji, J. Wang, and W. Liu, "Fiber-Reinforced Phthalonitrile Composites," in *Phthalonitrile Resins and Composites*, 2018, pp. 241–294. doi: 10.1016/B978-0-12-812966-1.00005-6.

[23] C. H. Zweben, "Composites: Overview," F. Bassani, G. L. Liedl, and P. B. T.-

E. of C. M. P. Wyder, Eds. Oxford: Elsevier, 2005, pp. 192–208. doi: https://doi.org/10.1016/B0-12-369401-9/00545-3.

[24] B. Fei, “2 - High-performance fibers for textiles,” in *The Textile Institute Book Series*, M. Miao and J. H. B. T.-E. of H.-P. T. Xin, Eds. Woodhead Publishing, 2018, pp. 27–58. doi: https://doi.org/10.1016/B978-0-08-101273-4.00002-0.

[25] S. J. Park and M. K. Seo, *Element and Processing*, vol. 18. 2011. doi: 10.1016/B978-0-12-375049-5.00006-2.

[26] M. C. Tanzi, S. Farè, and G. Candiani, “Chapter 1 - Organization, Structure, and Properties of Materials,” M. C. Tanzi, S. Farè, and G. B. T.-F. of B. E. Candiani, Eds. Academic Press, 2019, pp. 3–103. doi: https://doi.org/10.1016/B978-0-08-101034-1.00001-3.

[27] S. L. Ogin, P. Brøndsted, and J. Zangenberg, “1 - Composite materials: constituents, architecture, and generic damage,” in *Woodhead Publishing Series in Composites Science and Engineering*, R. Talreja and J. B. T.-M. D. Varna Fatigue and Failure of Composite Materials, Eds. Woodhead Publishing, 2016, pp. 3–23. doi: https://doi.org/10.1016/B978-1-78242-286-0.00001-7.

[28] A. K. Sharma, R. Bhandari, A. Aherwar, and R. Rimašauskiene, “Matrix materials used in composites: A comprehensive study,” in *Materials Today: Proceedings*, 2020, vol. 21, pp. 1559–1562. doi: 10.1016/j.matpr.2019.11.086.

[29] Q. H. Qin, “Introduction to the composite and its toughening mechanisms,” in *Toughening Mechanisms in Composite Materials*, Elsevier Inc., 2015, pp. 1–32. doi: 10.1016/B978-1-78242-279-2.00001-9.

[30] A. Afzal and Y. Nawab, “5 - Polymer composites,” in *Woodhead Publishing Series in Composites Science and Engineering*, Y. Nawab, S. M. Sapuan, and K. B. T.-C. S. for B. Shaker, Eds. Woodhead Publishing, 2021, pp. 139–152. doi:

https://doi.org/10.1016/B978-0-12-821984-3.00003-6.

[31] A. Shojaei and S. S. Khasraghi, “Chapter 13 - Self-healing and self-sensing smart polymer composites,” I.-M. Low and Y. B. T.-C. M. Dong, Eds. Elsevier, 2021, pp. 307–357. doi: https://doi.org/10.1016/B978-0-12-820512-9.00015-0.

[32] S. R. Sandler and W. Karo, “Chapter 3 - Epoxy Resins,” S. R. Sandler and W. B. T.-P. S. (Second E. Karo, Eds. San Diego: Academic Press, 1994, pp. 87–128. doi: https://doi.org/10.1016/B978-0-08-092555-4.50007-4.

[33] N. J. L. Megson, “Epoxide resins,” *Nature*, vol. 177, no. 4517, pp. 962–964, 1956, doi: 10.1038/177962a0.

[34] A. P. B. T.-I. to A. M. Mouritz, Ed., “13 - Polymers for aerospace structures,” Woodhead Publishing, 2012, pp. 268–302. doi: https://doi.org/10.1533/9780857095152.268.

[35] J. L. MASSINGILL and R. S. BAUER, “EPOXY RESINS,” C. D. Craver and C. E. B. T.-A. P. S. 21st C. Carraher, Eds. Oxford: Pergamon, 2000, pp. 393–424. doi: https://doi.org/10.1016/B978-008043417-9/50023-4.

[36] G. Gibson, “Epoxy Resins,” in *Brydson’s Plastics Materials: Eighth Edition*, Elsevier Inc., 2017, pp. 773–797. doi: 10.1016/B978-0-323-35824-8.00027-X.

[37] K. Hodd, “37 - Epoxy Resins,” G. Allen and J. C. B. T.-C. P. S. and S. Bevington, Eds. Amsterdam: Pergamon, 1989, pp. 667–699. doi: https://doi.org/10.1016/B978-0-08-096701-1.00178-6.

[38] N. Hashim, D. L. A. Majid, D. M. Baitab, N. Yidris, and R. Zahari, “Tensile Properties of Woven Intra-Ply Carbon/Kevlar Reinforced Epoxy Hybrid Composite at Sub-Ambient Temperature,” *Encycl. Mater. Compos.*, pp. 766–773, 2019, doi: 10.1016/B978-0-12-803581-8.11567-X.

[39] N. Sirosh, “FUELS – HYDROGEN STORAGE | Compressed,” J. B. T.-E. of E.

P. S. Garche, Ed. Amsterdam: Elsevier, 2009, pp. 414–420. doi: https://doi.org/10.1016/B978-044452745-5.00322-1.

[40] A. Fradet and P. Arlaud, “19 - Unsaturated Polyesters,” G. Allen and J. C. B. T.-C. P. S. and S. Bevington, Eds. Amsterdam: Pergamon, 1989, pp. 331–344. doi: https://doi.org/10.1016/B978-0-08-096701-1.00160-9.

[41] J. M. Kenny and L. Nicolais, “18 - Science and Technology of Polymer Composites,” G. Allen and J. C. B. T.-C. P. S. and S. Bevington, Eds. Amsterdam: Pergamon, 1989, pp. 471–525. doi: https://doi.org/10.1016/B978-0-08-096701-1.00236-6.

[42] S. J. Hosseinipour and G. H. Daneshi, “Energy absorbtion and mean crushing load of thin-walled grooved tubes under axial compression,” *Thin-Walled Struct.*, vol. 41, no. 1, pp. 31–46, 2003, doi: 10.1016/S0263-8231(02)00099-X.

[43] R. T. Leon and G. G. Deierlein, “Considerations for the Use of Quasi-Static Testing,” *Earthq. Spectra*, vol. 12, no. 1, pp. 87–109, Feb. 1996, doi: 10.1193/1.1585869.

[44] M. Alkateb, S. Sapuan, Z. Leman, M. Jawaid, and M. Ishak, “Quasi-static crush behaviour of environmentally friendly kenaf/wool epoxy composites elliptical tube,” *J. Mech. Eng. Sci.*, vol. 12, pp. 3671–3688, Jun. 2018, doi: 10.15282/jmes.12.2.2018.13.0325.

[45] S. Ramakrishna and H. Hamada, “Energy Absorption Characteristics of Crash Worthy Structural Composite Materials,” *Key Eng. Mater.*, vol. 141–143, no. 143 PART II, pp. 585–622, 1998, doi: 10.4028/WWW.SCIENTIFIC.NET/KEM.141-143.585.

[46] Y. Xiang, T. Yu, and L. Yang, “Comparative analysis of energy absorption capacity of polygonal tubes, multi-cell tubes and honeycombs by utilizing key

performance indicators," *Mater. Des.*, vol. 89, pp. 689–696, Jan. 2016, doi: 10.1016/J.MATDES.2015.10.004.

[47] S. E. Alkhatib, M. S. Matar, F. Tarlochan, O. Laban, A. S. Mohamed, and N. Alqwasmi, "Deformation modes and crashworthiness energy absorption of sinusoidally corrugated tubes manufactured by direct metal laser sintering," *Eng. Struct.*, vol. 201, p. 109838, Dec. 2019, doi: 10.1016/J.ENGSTRUCT.2019.109838.

[48] I. Duarte, L. Krstulović-Opara, J. Dias-de-Oliveira, and M. Vesenjak, "Axial crush performance of polymer-aluminium alloy hybrid foam filled tubes," *Thin-Walled Struct.*, vol. 138, pp. 124–136, May 2019, doi: 10.1016/J.TWS.2019.01.040.

[49] X. Cao, S. Duan, J. Liang, W. Wen, and D. Fang, "Mechanical properties of an improved 3D-printed rhombic dodecahedron stainless steel lattice structure of variable cross section," *Int. J. Mech. Sci.*, vol. 145, pp. 53–63, Sep. 2018, doi: 10.1016/J.IJMECSCI.2018.07.006.

[50] A. G. Mamalis, M. Robinson, D. E. Manolakos, G. A. Demosthenous, M. B. Ioannidis, and J. Carruthers, "Crashworthy capability of composite material structures," *Compos. Struct.*, vol. 37, no. 2, pp. 109–134, Feb. 1997, doi: 10.1016/S0263-8223(97)80005-0.

[51] J. J. Carruthers, A. P. Kettle, and A. M. Robinson, "Energy Absorption Capability and Crashworthiness of Composite Material Structures: A Review," *Appl. Mech. Rev.*, vol. 51, no. 10, pp. 635–649, Oct. 1998, doi: 10.1115/1.3100758.

[52] S. S. Reddy, C. Yuvraj, and K. P. Rao, "Design, Analysis, Fabrication and Testing of CFRP with CNF Composite Cylinder for Space Applications," *Int. J.*

Compos. Mater., vol. 5, no. 5, pp. 102–128, 2015, doi: 10.5923/j.cmaterials.20150505.03.

[53] G. L. Farley, "The Effects of Crushing Speed on the Energy-Absorption Capability of Composite Tubes," *J. Compos. Mater.*, vol. 25, no. 10, pp. 1314–1329, Jul. 1991, doi: 10.1177/002199839102501004.

[54] G. Zhu, G. Sun, Q. Liu, G. Li, and Q. Li, "On crushing characteristics of different configurations of metal-composites hybrid tubes," *Compos. Struct.*, vol. 175, pp. 58–69, Sep. 2017, doi: 10.1016/J.COMPSTRUCT.2017.04.072.

[55] I. Sigalas, M. Kumosa~, and D. Hull, "Trigger Mechanisms in Energy-Absorbing Glass Cloth/Epoxy Tubes," *Compos. Sci. Technol.*, vol. 40, pp. 265–287, 1991.

[56] D. W. Schmueser and L. E. Wickliffe, "Impact Energy Absorption of Continuous Fiber Composite Tubes," *J. Eng. Mater. Technol.*, vol. 109, no. 1, pp. 72–77, Jan. 1987, doi: 10.1115/1.3225937.

[57] J. Berry and D. Hull, "Effect of speed on progressive crushing of epoxy-glass cloth tubes," in *Conf. Ser. Inst. Phys*, 1984, vol. 70, pp. 463–470.

[58] K. C. Shin, J. J. Lee, K. H. Kim, M. C. Song, and J. S. Huh, "Axial crush and bending collapse of an aluminum/GFRP hybrid square tube and its energy absorption capability," *Compos. Struct.*, vol. 57, no. 1–4, pp. 279–287, Jul. 2002, doi: 10.1016/S0263-8223(02)00094-6.

[59] P. H. Thornton, "The Crush Behavior of Pultruded Tubes at High Strain Rates," *J. Compos. Mater.*, vol. 24, no. 6, pp. 594–615, Jul. 1990, doi: 10.1177/002199839002400602.

[60] A. B. M. Supian, S. M. Sapuan, M. Y. M. Zuhri, E. S. Zainudin, and H. H. Ya, "Crashworthiness performance of hybrid kenaf/glass fiber reinforced epoxy tube

on winding orientation effect under quasi-static compression load," *Def. Technol.*, vol. 16, no. 5, pp. 1051–1061, Oct. 2020, doi: 10.1016/j.dt.2019.11.012.

[61] H. Hamada and S. Ramakrishna, "Impact performance of glass cloth/epoxy composite tubes with different surface treatment," *Compos. Interfaces*, vol. 4, no. 1, pp. 35–44, Jan. 1996, doi: 10.1163/156855496X00137.

[62] G. Sun, Z. Wang, J. Hong, K. Song, and Q. Li, "Experimental investigation of the quasi-static axial crushing behavior of filament-wound CFRP and aluminum/CFRP hybrid tubes," *Compos. Struct.*, vol. 194, pp. 208–225, Jun. 2018, doi: 10.1016/J.COMPSTRUCT.2018.02.005.

[63] H. Hamada, J. C. Coppola, D. Hull, Z. Maekawa, and H. Sato, "Comparison of energy absorption of carbon/epoxy and carbon/PEEK composite tubes," *Composites*, vol. 23, no. 4, pp. 245–252, Jul. 1992, doi: 10.1016/0010-4361(92)90184-V.

[64] A. M. Elgalai, E. Mahdi, A. M. S. Hamouda, and B. S. Sahari, "Crushing response of composite corrugated tubes to quasi-static axial loading," *Compos. Struct.*, vol. 66, no. 1–4, pp. 665–671, Oct. 2004, doi: 10.1016/J.COMPSTRUCT.2004.06.002.

[65] L. N. S. Chiu *et al.*, "Crush responses of composite cylinder under quasi-static and dynamic loading," *Compos. Struct.*, vol. 131, pp. 90–98, Nov. 2015, doi: 10.1016/J.COMPSTRUCT.2015.04.057.

[66] E. Mahdi and T. A. Sebaey, "An experimental investigation into crushing behavior of radially stiffened GFRP composite tubes," *Thin-Walled Struct.*, vol. 76, pp. 8–13, Mar. 2014, doi: 10.1016/J.TWS.2013.10.018.